



# Decentralized Simultaneous Multi-target Exploration using a Connected Network of Multiple Robots

Thomas Nestmeyer, Paolo Robuffo Giordano, Heinrich H. Bühlhoff, Antonio Franchi

## ► To cite this version:

Thomas Nestmeyer, Paolo Robuffo Giordano, Heinrich H. Bühlhoff, Antonio Franchi. Decentralized Simultaneous Multi-target Exploration using a Connected Network of Multiple Robots. *Autonomous Robots*, 2017, 41 (4), pp.989-1011. 10.1007/s10514-016-9578-9 . hal-01332937

**HAL Id: hal-01332937**

**<https://inria.hal.science/hal-01332937>**

Submitted on 16 Jun 2016

**HAL** is a multi-disciplinary open access archive for the deposit and dissemination of scientific research documents, whether they are published or not. The documents may come from teaching and research institutions in France or abroad, or from public or private research centers.

L'archive ouverte pluridisciplinaire **HAL**, est destinée au dépôt et à la diffusion de documents scientifiques de niveau recherche, publiés ou non, émanant des établissements d'enseignement et de recherche français ou étrangers, des laboratoires publics ou privés.

# Decentralized Simultaneous Multi-target Exploration using a Connected Network of Multiple Robots

Thomas Nestmeyer · Paolo Robuffo Giordano · Heinrich H. Bühlhoff · Antonio Franchi

the date of receipt and acceptance should be inserted later

**Abstract** This paper presents a novel decentralized control strategy for a multi-robot system that enables parallel multi-target exploration while ensuring a time-varying connected topology in cluttered 3D environments. Flexible continuous connectivity is guaranteed by building upon a recent connectivity maintenance method, in which limited range, line-of-sight visibility, and collision avoidance are taken into account at the same time. Completeness of the decentralized multi-target exploration algorithm is guaranteed by dynamically assigning the robots with different motion behaviors during the exploration task. One major group is subject to a suitable downscaling of the main traveling force based on the traveling efficiency of the current leader and the direction alignment between traveling and connectivity force. This supports the leader in always reaching its current target and, on a larger time horizon, that the whole team realizes the overall task in finite time. Extensive Monte Carlo simulations with a group of several quadrotor UAVs show the scalability and effectiveness of the proposed method and experiments validate its practicability.

**Keywords** multi-robot coordination · path-planning · decentralized exploration · connectivity maintenance

## 1 Introduction

Success of multi-robot systems is based on their ability of parallelizing the execution of several small tasks composing a larger complex mission such as, for instance, the inspection of a certain number of locations either generated off- or online during the robot motion (e.g., exploration, data collection, surveillance, large-scale medical supply or search and rescue (Howard et al. 2006; Franchi et al. 2009; Pasqualetti et al. 2012; Murphy et al. 2008; Faigl and Hollinger 2014)). In all these cases, a fundamental difference between a group of many single robots and a multi-robot system is the ability to communicate (either explicitly or implicitly) in order to then cooperate together towards a common objective. Another distinctive characteristic in multi-robot systems is the absence of central planning units, as well as all-to-all communication infrastructures, leading to a *decentralized* approach for algorithmic design and implementations (Lynch 1997). While communication of a robot with every other robot in the group (via multiple hops) would still be possible as long as the group stays connected, in a decentralized approach each robot is only assumed able to communicate with the robots in its 1-hop neighborhood (i.e., typically the ones spatially close by). This brings the advantage of scalability in communication and computation complexity when considering groups of many robots.

The possibility for every robot to share information (via, possibly, multiple hops/iterations) with any other robot in the group is a basic requirement for typical multi-robot algorithms and, as well-known, it is

---

T. Nestmeyer - E-mail: tnestmeyer@tue.mpg.de  
Max Planck Institute for Intelligent Systems,  
Spemannstraße 41, 72076 Tübingen, Germany

P. Robuffo Giordano - E-mail: prg@irisa.fr  
CNRS at Irisa and Inria Rennes Bretagne Atlantique,  
Campus de Beaulieu, 35042 Rennes cedex, France

H. H. Bühlhoff - E-mail: hhb@tuebingen.mpg.de  
Max Planck Institute for Biological Cybernetics,  
Spemannstraße 38, 72076 Tübingen, Germany

A. Franchi - E-mail: antonio.franchi@laas.fr  
CNRS, LAAS, 7 Av. du Colonel Roche, F-31400 Toulouse, France  
and Univ de Toulouse, LAAS, F-31400 Toulouse, France

Simulations and experiments were performed while the authors were at the MPI for Biological Cybernetics, Tübingen, Germany.

directly related to the connectivity of the underlying *graph* modeling inter-robot interactions. Graph connectivity is a prerequisite to properly fuse the information collected by each robot, e.g., for mapping, localization, and for deciding the next actions to be taken. Additionally, many distributed algorithms like consensus (Olfati-Saber and Murray 2004) and flooding (Lim and Kim 2001) require a connected graph for their successful convergence. Preserving graph connectivity during the robot motion is, thus, a fundamental requirement; however, connectivity maintenance may not be a trivial task in many situations, e.g., because of limited capabilities of onboard sensing/communication devices which can be hindered by constraints such as occlusions or maximum range. Given the cardinal role of communication for the successful operation of a multi-robot team, it is then not surprising that a substantial effort has been spent over the last years for devising strategies able to preserve graph connectivity despite constraints in the inter-robot sensing/communication possibilities, see, e.g., Antonelli et al. (2005); Stump et al. (2008, 2011); Pei and Mutka (2012); Robuffo Giordano et al. (2013). In general, *fixed topology* methods represent conservative strategies that achieve connectivity maintenance by restraining any pairwise link of the interaction graph to be broken during the task execution. A different possibility is to aim for *periodical connectivity* strategies, where each robot can remain separated from the group during some period of time for then re-joining when necessary. *Continuous connectivity* methods instead try to obtain maximum flexibility (links can be continuously broken and restored unlike in the fixed topology cases) while preserving at any time the fundamental ability for any two nodes in the group to share information via a (possibly multi-hop) path (unlike in periodical connectivity methods).

With respect to this state-of-the-art, the problem tackled by this paper is the design of a *multi-target* exploration/visiting strategy for a team of mobile robots in a cluttered environment able to *i)* allow visiting multiple targets at once (for increasing the efficiency of the exploration), while *ii)* always guaranteeing connectivity maintenance of the group despite some typical sensing/communication constraints representative of real-world situations, *iii)* without requiring presence of central nodes or processing units (thus, developing a fully *decentralized* architecture), and *iv)* without requiring that all the targets are known at the beginning of the task (thus, considering *online target generation*).

Designing a decentralized strategy that combines multi-target exploration and continuous connectivity maintenance is not trivial as these two goals impose often antithetical constraints. Several attempts have in-

deed been presented in the previous literature: a *fixed-topology* and centralized method is presented in Antonelli et al. (2005), which, using a virtual chain of mobile antennas, is able to maintain the communication link between a ground station and a single mobile robot visiting a given sequence of target points. The method is further refined in Antonelli et al. (2006). A similar problem is addressed in Stump et al. (2008) by resorting to a partially centralized method where a linear programming problem is solved at every step of motion in order to mix the derivative of the second smallest eigenvalue of a weighted Laplacian (also known as algebraic connectivity, or Fiedler eigenvalue) and the *k*-connectivity of the system. A line-of-sight communication model is considered in Stump et al. (2011), where a centralized approach, based on polygonal decomposition of the known environment, is used to address the problem of deploying a group of roving robots while achieving *periodical connectivity*. The case of periodical connectivity is also considered in Pasqualetti et al. (2012) and Hollinger and Singh (2012). The first paper optimally solves the problem of patrolling a set of points to be visited as often as possible. The second presents a heuristic algorithm exploiting the concept of implicit coordination. *Continuous connectivity* between a group of robots exploring an unknown 2D environment and a single base station is considered in Pei et al. (2010). The proposed exploration methodology, similar to the one presented in Franchi et al. (2009), is integrated with a centralized algorithm running on the base station and solving a variant of the Steiner Minimum Tree Problem. An extension of this approach to heterogeneous teams is presented in Pei and Mutka (2012). Zavlanos and Pappas (2007) exploit a potential field approach to keep the second smallest eigenvalue of the Laplacian positive. The method is tested with ground robots in an empty environment and assumes that each robot has access to the whole formation for computing the connectivity eigenvalue and the associated potential field. It is therefore not scalable, because the strength of all links has to be broadcasted to all robots in the group. Continuous connectivity achieved by suitable mission planning is described in Mosteo et al. (2008), although this work does not allow for parallel exploration. Another method providing flexible connectivity based on a spring-damper system, but not able to handle significant obstacles, is reported in Tardioli et al. (2010).

A decentralized strategy addressing the problem of continuous connectivity maintenance for a multi-robot team is considered in Robuffo Giordano et al. (2013). In this latter work, the introduction of a sensor-based weighted Laplacian allows to distributively and analytically compute the anti-gradient of a generalized Fiedler

eigenvalue. The connectivity maintenance action is further embedded with additional constraints and requirements such as inter-robot and obstacle collision avoidance, and a stability guarantee of the whole system, when perturbed by external control inputs for steering the whole formation, is also provided. Finally, apart for Robuffo Giordano et al. (2013), all the previously mentioned continuous connectivity methods have only been applied to 2D-environment models.

In this work, we leverage upon the general decentralized strategy for connectivity maintenance of Robuffo Giordano et al. (2013) for proposing a solution to the aforementioned problem of decentralized *multi-target exploration* while coping with the (possibly opposing) constraints of continuous connectivity maintenance in a cluttered 3D environment. The main contributions of this paper and features of the proposed algorithm can then be summarized as follows: *i)* decentralized and continuous maintenance of connectivity, *ii)* guarantee of collision avoidance with obstacles and among robots, *iii)* possibility to take into account non-trivial sensing/communication models, including maximum range and line-of-sight visibility in 3D, *iv)* stability of the overall multi-robot dynamical system, *v)* decentralized exploration capability, *vi)* possibility for more than one robot to visit different targets at the same time, *vii)* on-line path planning without the need for any (centralized) pre-planning phase, *viii)* applicability to both 2D and 3D cluttered environments, and finally *ix)* completeness of the multi-target exploration (i.e., all robots are guaranteed to reach all their targets in a finite time). The items *i)* - *iv)* have already been tackled in Robuffo Giordano et al. (2013) and are here taken as a basis for our work. On the other hand, the combination of *i)* - *iv)* with the items *v)* - *ix)* is a novel contribution: to the best of our knowledge, our work is then the first attempt to propose a decentralized multi-target exploration algorithm possessing all the mentioned features altogether.

The rest of the paper is organized as follows: Sec. 2 provides a formal description of the problem under consideration. The proposed algorithm is then thoroughly illustrated in Sec. 3. In Sec. 4, we report the results of extensive Monte Carlo simulations and experiments with real quadrotors, and Sec. 5 concludes the paper. Finally, we recap in Appendix A the main features of the decentralized continuous connectivity method presented in Robuffo Giordano et al. (2013) which is extensively exploited in this paper. We finally note that a preliminary version of our work has been presented in Nestmeyer et al. (2013a,b).

## 2 System Model and Problem Setting

We consider a group of  $N$  robots operating in a 3D obstacle-populated environment and denote with  $q_i \in \mathbb{R}^3$  the position of a reference point of the  $i$ -th robot,  $i = 1, \dots, N$ , in an inertial world frame. We also let  $\mathcal{O}$  be the set of obstacle points in the environment. Each robot  $i$  is assumed to be endowed with the relative position  $q_j - q_i$  of another robot  $j$  provided that:

1.  $\|q_j - q_i\| < R_s$ , where  $R_s > 0$  is the maximum sensing range of the sensor, and
2.  $\min_{\varsigma \in [0,1], o \in \mathcal{O}} \|q_i + \varsigma(q_j - q_i) - o\| \geq R_o$ , i.e., the line segment connecting  $q_i$  to  $q_j$  is at least at distance  $R_o > 0$  away from any obstacle point.

These two conditions account for two common characteristics of exteroceptive sensors, namely, presence of a limited sensing range  $R_s$ , and the need for a non-occluded line-of-sight visibility<sup>1</sup>. We further assume that if the  $i$ -th robot can measure  $q_j - q_i$  then it can also communicate with the  $j$ -th robot, that is, the sensing and communication graphs are taken coincident. This assumption is justified by the fact that communication typically relies on wireless technology, thus with a broader range than sensing and without the need for direct visibility to operate. The neighbors of the  $i$ -th robot are denoted with  $\mathcal{N}_i(t)$ , i.e., the (time-varying) set of robots whose relative position can be measured by the  $i$ -th robot at time  $t$ .

Each robot  $i$  is also endowed with a sensor that measures the relative position  $o - q_i$  of every obstacle point  $o \in \mathcal{O}$  such that  $\|o - q_i\| < R_m$ , where  $R_m > 0$  is the maximum sensing range of this sensor.

Consider the time-varying (undirected) *interaction graph* defined as  $\mathcal{G}(t) = (\mathcal{V}, \mathcal{E}(t))$ , where  $\mathcal{V} = \{1, \dots, N\}$  and  $\mathcal{E}(t) = \{(i, j) \mid j \in \mathcal{N}_i(t)\}$ . Preserving connectivity of  $\mathcal{G}(t)$  for all  $t$ , allows every robot to communicate *at any time* with any other robot in the network by means of a suitable multi-hop routing strategy, although due to efficiency and scalability reasons, it is always preferred to use one-hop communication when possible.

As previously stated, decentralized continuous connectivity maintenance is guaranteed by exploiting the method described in Robuffo Giordano et al. (2013), which is based on a gradient-descent action that keeps positive the second smallest eigenvalue  $\lambda_2$  of the *sensor-based* weighted graph Laplacian (Fiedler 1973) (see Appendix A for a formal definition).

Each  $i$ -th robot is finally endowed with a local motion controller able to let  $q_i$  track any arbitrary desired

<sup>1</sup> More complex sensing models could also be taken into account, see Robuffo Giordano et al. (2013) for a discussion in this sense.

$\bar{\mathcal{C}}^2$  trajectory  $q_i(t)$  with a sufficiently small tracking error. This is again a well-justified assumption for almost all mobile robotic platforms of interest, and its validity will also be supported by the experimental results of Sec. 4.2. Following the control framework introduced in Robuffo Giordano et al. (2013), the dynamics of  $q_i$  is then modeled as the following second order system

$$\Sigma : \begin{cases} M_i \dot{v}_i - f_i^B - f_i^\lambda = f_i \\ \dot{q}_i = v_i \end{cases} \quad i = 1, \dots, N \quad (1)$$

where  $v_i \in \mathbb{R}^3$  is the robot velocity,  $M_i \in \mathbb{R}^{3 \times 3}$  is its positive definite inertia matrix, and:

1.  $f_i^B = -B_i v_i \in \mathbb{R}^3$  is the *damping force* (with  $B_i \in \mathbb{R}^{3 \times 3}$  being a positive definite damping matrix) meant to represent both typical friction phenomena (e.g., wind/atmosphere drag in the case of aerial robots) and/or a stabilizing control action;
2.  $f_i^\lambda \in \mathbb{R}^3$  is the *generalized connectivity force* whose decentralized computation and properties are thoroughly described in Robuffo Giordano et al. (2013) (a short recap is provided in Appendix A);
3.  $f_i \in \mathbb{R}^3$  is the *traveling force* used to actually steer the robot motion in order to execute the given task. An appropriate design of  $f_i$  is the main goal of this work. As will be clear in the following, special care must to be taken in the design of  $f_i$  to avoid, for instance, deadlocks situations in which the robot group ‘gets stuck’.

The following fact, shown in Robuffo Giordano et al. (2013) and recalled in Appendix A, holds:

**Fact 1.** *As long as  $f_i$  keeps bounded, the action of the generalized connectivity force  $f_i^\lambda$  will always ensure obstacle and inter-robot collision avoidance and continuous connectivity maintenance for the graph  $\mathcal{G}(t)$  despite the various sensing/communication constraints (in the worst case, by completely dominating the bounded  $f_i$ ).*

## 2.1 Multi-target Exploration Problem

We consider the broad class of problems in which each robot runs a black-boxed algorithm that produces *online*<sup>2</sup> a list of targets that have to be visited by the robot in the presented order. We refer to this algorithm as the *target generator* of the  $i$ -th robot, and we also assume that the portion of the map needed

<sup>2</sup> By *online* we mean that the targets are generated at runtime, thus precluding the presence of a preliminary phase in which the robots may *plan in advance* the multi-target exploration action. Indeed, if all the targets are known beforehand, one could still apply our method but other planning strategies might potentially lead to better solutions.

to reach the next location from the current position  $q_i$  is known to robot  $i$ . The target generator may represent a large variety of algorithms, such as pursuit-evasion (Durham et al. 2012), patrolling (Pasqualetti et al. 2012), exploration/mapping (Franchi et al. 2009; Burgard et al. 2005), mobile-ad-hoc-networking (Antonelli et al. 2005), and active localization (Jensfelt and Kristensen 2001). It might be a cooperative algorithm, or each robot could have a target generator with objectives that are independent from the other target generators. Another possibility is to appoint a human supervisor as the target generator.

Depending on the particular application, the locations in the lists provided online by the target generators may, e.g., represent:

1. view-points from where to perform the sensorial acquisitions,
2. coordinates of objects that have to be picked up or dropped down,
3. positions of some base stations located in the environment.

We formally denote with  $(z_i^1, \dots, z_i^{m_i}) \in \mathbb{R}^{3 \times m_i}$  the list of  $m_i$  locations provided by the  $i$ -th target generator. Additionally, we consider the possibility, for the target generator, to specify a time duration  $\Delta t_i^k < \infty$  for which the  $i$ -th robot is required to stay close to the point  $z_i^k$ , with  $k = 1, \dots, m_i$ . This quantity may represent, with reference to the previous examples, the time

1. needed to perform a full sensorial acquisition,
2. necessary to pick up/drop down an object,
3. required to upload/download some information from a base station,

Finally, we also introduce the concept of a *cruise speed*  $v_i^{\text{cruise}} > 0$  that should be maintained by the  $i$ -th robot during the transfer phase from a point to the next one.

Given these modeling assumptions, the problem addressed in this paper can be formulated as follows:

**Problem 1.** *Given a sequence of targets  $z_i^1, \dots, z_i^{m_i}$  (presented online) for every robot  $i = 1, \dots, N$ , together with the corresponding sequence of time durations  $\Delta t_i^1, \dots, \Delta t_i^{m_i}$  and a radius  $R_z$ , design, for every  $i = 1, \dots, N$ , a decentralized feedback control law  $f_i$  (i.e., a function using only information locally and 1-hop available to the  $i$ -th robot) for system (1) which is bounded and such that, for the closed-loop trajectory  $q_i(t, f_i, [0, t])$ , there exists a time sequence  $0 < t_i^1 < \dots < t_i^{m_i} < \infty$  so that for all  $k = 1 \dots m_i$ , robot  $i$  remains for the duration  $\Delta t_i^k$  within a ball of radius  $R_z$  centered at  $z_i^k$ , formally  $\forall t \in [t_i^k, t_i^k + \Delta t_i^k] : \|q_i(t) - z_i^k\| < R_z$ .*

Table 1: Meaning of the variable names.

variable	meaning
$N$	number of robots
$q_i$	position of $i$ -th robot
$v_i$	velocity of $i$ -th robot
$\mathcal{O}$	set of obstacle points
$R_s$	maximum sensing range
$R_o$	minimum distance to obstacle
$R_c$	minimum inter-robot distance
$\mathcal{N}_i$	neighbors of $i$ -th robot
$\mathcal{G}$	interaction graph
$\lambda_2$	second smallest eigenvalue of the sensor-based weighted graph Laplacian
$f_i^\lambda$	generalized connectivity force
$f_i^B$	damping force
$f_i$	traveling force
$z_i^k$	$k$ -th target of $i$ -th robot
$\Delta t_i^k$	amount of time to stay close to target $z_i^k$
$R_z$	maximum distance to target when anchored
$v_i^{\text{cruise}}$	maximum cruise speed
$\gamma_i$	path to current target, starting from position of robot at time of computation
$q_i^\gamma$	closest point of path from current position
$d_i^\gamma$	length of remaining path
$R_\gamma$	distance to path at which it should be re-planned
$\alpha_A$	weighting of position vs. velocity error
$e_i$	absolute tracking error of $i$ -th robot along path
$(x_c, x_M)$	tracking error bounds for the traveling efficiency
$\Lambda_i$	traveling efficiency of $i$ -th robot (i.e., tracking error nonlinearly scaled to $[0, 1]$ based on $x_c, x_M$ )
$\hat{\Lambda}_p^i$	estimation of the traveling efficiency of the ‘prime traveler’ by the $i$ -th robot
$\Theta_i$	force direction alignment between connectivity and traveling force of $i$ -th robot
$\sigma$	weighting between the force direction alignment and the ‘prime traveler’ traveling efficiency
$\rho_i$	downscaling factor of a ‘secondary traveler’, dependent on $\hat{\Lambda}_p^i$ , $\Theta_i$ and $\sigma$

### 3 Decentralized Algorithm

In this section, we describe the proposed distributed algorithm aimed at generating a traveling force  $f_i$  that solves Problem 1. We note that the design of such an autonomous distributed algorithm requires special care: When added to the generalized connectivity force in (1), the traveling force  $f_i$  should fully exploit the group capabilities to concurrently visit the targets of all robots whenever possible and, at the same time, should not lead to ‘*local minima*’, where the robots get stuck, due to the simultaneous presence of the hard connectivity constraint. While Robuffo Giordano et al. (2013) already gave an exact description of  $f_i^B$  and  $f_i^\lambda$ , an application of  $f_i$  was kept open. The main focus of this work is to define  $f_i$  in such a way that the above mentioned challenges are properly addressed.

In order to provide an overview of the several variables used in Secs. 2 and 3, we included Table 1 for the reader’s convenience.

#### 3.1 Notation and Algorithm Overview

As in any distributed design, several instances of the proposed algorithms run separately on each robot and locally exchange information with the ‘neighboring’ instances via communication. Each instance is split into two concurrent routines: a *planning algorithm* and a *motion control algorithm* whose pseudocodes are given in Algorithm 1 and Algorithm 2, respectively. The planning algorithm acts at a higher level and performs the following actions:

- it processes the targets provided by the target generator,
- it generates the desired path to the current target, and
- it selects an appropriate motion control behavior (see later).

The motion control algorithm acts at a lower level by specifying the traveling force  $f_i$  as a function of the behavior and the planned path selected by the planning algorithm<sup>3</sup>.

The two algorithms have access to the same variables which are formally introduced as follows (see Fig. 1 for a graphical representation of some of these variables): the variable `targetQueuei` is filled online by the target generator and contains a list of future targets to be visited by the  $i$ -th robot. During the overall running time of the algorithms, the target generator of robot  $i$  has access to the whole list `targetQueuei`. The current target for the  $i$ -th robot (i.e., the last target extracted from the first entry in `targetQueuei`) is denoted with  $z_i$ . Variable  $\gamma_i$  is a  $\bar{C}^2$  geometric path that leads from the current position  $q_i$  of the  $i$ -th robot to the target  $z_i$ . In our implementation, we used B-splines (Biagiotti and Melchiorri 2008) in order to get a parameterized smooth path, but any other  $\bar{C}^2$  path would be appropriate. If the robot is not traveling towards any target, then  $\gamma_i$  is set to `null`.

With reference to Fig. 1, we also denote with  $q_i^\gamma$  the closest point of the path  $\gamma_i$  to  $q_i$ , i.e., the solution of  $\arg \min_{p \in \gamma_i} \|p - q_i\|$ . The portion of the path  $\gamma_i$  from  $q_i^\gamma$  to  $z_i$  is referred to as the *remaining path*, and its length is denoted with  $d_i^\gamma$ .

The motion behavior of the  $i$ -th robot is determined by the variable `statei` that can take four possible values:

- `connector`
- `prime-traveler`
- `secondary-traveler`
- `anchor`.

<sup>3</sup> The two routines can run at two different frequencies, typically slower for the planning loop and faster for the motion control loop.

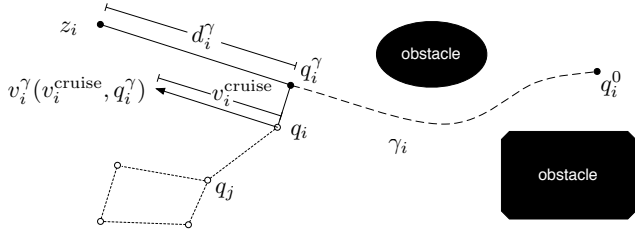


Fig. 1: Position  $q_i$  and path  $\gamma_i$  followed by a traveler from the point  $q_i^0$  to the current target  $z_i$ . The solid part of the path represents the *remaining path* which starts at the closest point on the path  $q_i^\gamma$  and whose length is denoted by  $d_i^\gamma$ .

The following provides a qualitative illustration of these motion behaviors, while a functional description is given in the next sections:

- *‘connector’*: a robot in this state is not assigned any target by the target generator and therefore, its only goal is to help keeping the graph  $\mathcal{G}$  connected. For this reason  $f_i$  is set to zero and hence the robot is subject solely to the damping and generalized connectivity force  $f_i^\lambda$  in (1);
- *‘prime traveler’*: a robot in this state travels towards its current target  $z_i$  along the path  $\gamma_i$  thanks to the force  $f_i$ . At the same time, the robot distributively broadcasts to every other robot a non-negative real number, denoted with  $\Lambda_i$ , that represents its *traveling efficiency*. It is essential for the algorithm that only one ‘prime traveler’ exists in the group at any time. Every other robot with an assigned target needs to be a ‘secondary traveler’ or ‘anchor’. This feature will allow one robot (the ‘prime traveler’) to reach its target with a high priority, while the other robots will only be allowed to reach their own targets as long as this action does not hinder the ‘prime traveler’ goal.
- *‘secondary traveler’*: a robot in this state travels towards its current target  $z_i$  along the path  $\gamma_i$  thanks to the force  $f_i$ . The robot keeps an internal estimation  $\hat{\Lambda}_p^i$  of the traveling efficiency of the current ‘prime traveler’, and it scales down the intensity of its traveling force  $f_i$  by an *adaptive gain*  $\rho_i$  whenever the action of  $f_i$  is ‘too conflicting’ w.r.t. that of  $f_i^\lambda$ , or the ‘prime traveler’  $\hat{\Lambda}_p^i$  drops lower than a given threshold.
- *‘anchor’*: a robot in this state has reached the proximity of the target  $z_i$ . The force  $f_i$  is then exploited in order to keep  $q_i$  within a circle of radius  $R_z$  centered at  $z_i$  (i.e., the robot is ‘anchored’ to the target), while waiting for the associated time  $\Delta t_i$  to elapse.

To summarize this qualitative description, these behaviors are designed in such a way that the single ‘prime traveler’ approaches its target with the highest priority, the ‘secondary travelers’ approach their targets as long

### Procedure Start-up for Robot $i$

---

```

1 if targetQueuei is empty then
2    $\gamma_i \leftarrow \text{null}$ 
3   statei  $\leftarrow$  connector
4 else
5   Extract first target from targetQueuei and save it as  $z_i$ 
6    $\gamma_i \leftarrow$  Shortest obstacle-free path from  $q_i$  to  $z_i$ 
7   Enroll in the list of Candidates to take part in the first
   distributed ‘prime traveler’ election
8   if  $i = \arg \min_{j \in \text{Candidates}} d_j^\gamma$  then
9     statei  $\leftarrow$  prime-traveler
10  else
11    statei  $\leftarrow$  secondary-traveler
12   $\hat{\Lambda}_p^i \leftarrow 0$ 
13 Run Algorithm 1 and Algorithm 2 in parallel

```

---

as they have enough spatial freedom by the generalized connectivity force, the ‘anchors’ stay close to the target until their task is completed, and the ‘connectors’ help the ‘secondary travelers’ in providing as much spatial freedom as possible while preserving the connectivity of the graph.

### 3.2 Start-up phase

The Procedure ‘Start-up for Robot  $i$ ’ performs the distributed initialization of the planning and motion control algorithms. Its pseudocode is quickly commented in the following.

At the beginning, if targetQueue<sub>i</sub> is empty then the path  $\gamma_i$  is set to **null** and state<sub>i</sub> to **connector** (line 3). Otherwise the first target from targetQueue<sub>i</sub> is extracted and saved in  $z_i$ . Then, the robot  $i$  computes a  $\bar{C}^2$  shortest and obstacle-free path  $\gamma_i$  that connects its current position  $q_i$  with  $z_i$  (line 6). This path is generated with a two-step optimization method: We note that, depending on the smoothing parameter, this approximation is not guaranteed to leave enough clearance from surrounding obstacles. Obstacle avoidance is nevertheless ensured thanks to the presence of the generalized connectivity force that prevents any possible collisions by (possibly) locally adjusting the planned path when needed. As an alternative, one could also rely on the method proposed in Masone et al. (2012) for directly generating a smooth path with enough clearance from obstacles.

Subsequently, the robot takes part in the distributed election of the first ‘prime traveler’ (see Sec. 3.3). Depending on the outcome of this election, state<sub>i</sub> is set either to **prime-traveler** or **secondary-traveler**.

At the end of the initialization procedure, the estimate  $\hat{\Lambda}_p^i$  of the traveling efficiency of the current ‘prime

traveler' is initialized to zero (line 12) for all robots, and the planning and motion control algorithms are both started (line 13).

### 3.3 Election of the 'prime traveler'

In a general election of a new 'prime traveler', the current 'prime traveler' triggers the election process (line 14 of Algorithm 1), to which every 'secondary traveler' replies with its index and remaining path length, in order to be taken into the list of candidates (line 23). Since this election is a low-frequency event, we chose to implement it via a simple flooding algorithm (Lim and Kim 2001). Although this solution complies with the requirement of being decentralized, one could also resort to 'smarter' distributed techniques such as (Lynch 1997). The 'prime traveler' then waits for  $2(N-1)$  steps to collect these replies, being  $2(N-1)$  the maximum number of steps needed to reach every robot with flooding and obtain a reply. The winner of this election is then the robot with the shortest remaining path length  $d_i^r$ , i.e., the robot solving  $\arg \min_{j \in \text{Candidates}} d_j^r$ . In the unlikely event of two (or more) robots having exactly the same remaining path length, the one with the lower index is elected. During the whole election process, the 'prime traveler' keeps its role and only upon decision it abdicates by switching into the 'anchor' state. After announcing the winner, no 'prime traveler' exists in the short time interval (at most  $N-1$  steps) until the announcement reaches the winning 'secondary traveler'. This winning robot then switches into the 'prime traveler' behavior. This mechanism makes sure that at most one 'prime traveler' exists at any given time.

The *first* election in the Start-up phase (see Sec. 3.2 and line 7 in Procedure 'Start-up for Robot  $i$ ') is handled slightly differently. Instead of the current 'prime traveler' organizing the election, robot 1 is always assigned the role of host and, instead of the only 'secondary travelers' replying, every robot with an assigned target replies with its index and remaining path length (including robot 1 if it has an assigned target).

### 3.4 Planning Algorithm

In this section, we describe in detail the execution of Algorithm 1 running on the  $i$ -th robot, whose logical flow is provided in Figure 2 as a graphical representation. The algorithm consists of a continuous loop where different decisions are taken according to the value of  $\text{state}_i$  and according to the following different behaviors:

---

#### Algorithm 1: Planning for Robot $i$

---

```

1 while true do
2   switch  $\text{state}_i$  do
3     case connector
4       if  $\text{targetQueue}_i$  is not empty then
5         Extract the next target from  $\text{targetQueue}_i$  and
          save it as  $z_i$ 
6          $\gamma_i \leftarrow$  Shortest obstacle-free path from  $q_i$  to  $z_i$ 
7         if There is no 'prime traveler' in the group then
8            $\text{state}_i \leftarrow$  prime-traveler
9         else
10           $\text{state}_i \leftarrow$  secondary-traveler
11      case prime-traveler
12        if  $\|q_i - z_i\| < R_z$  then
13           $\gamma_i \leftarrow$  null
14          Permit 'prime traveler' candidacy within timeout
15           $\text{state}_i \leftarrow$  anchor
16      case secondary-traveler
17        if  $\|q_i - q_i^\gamma\| > R_\gamma$  then
18           $\gamma_i \leftarrow$  Shortest obstacle-free path from  $q_i$  to  $z_i$ 
19        if  $\|q_i - z_i\| < R_z$  then
20           $\gamma_i \leftarrow$  null
21           $\text{state}_i \leftarrow$  anchor
22        else if 'prime traveler' candidacy is allowed then
23          Enroll in the list of Candidates to take part in
          the distributed 'prime traveler' election
24          if  $i = \arg \min_{j \in \text{Candidates}} d_j^r$  then
25             $\text{state}_i \leftarrow$  prime-traveler
26      case anchor
27        if task at target  $z_i$  is completed then
28           $\text{state}_i \leftarrow$  connector

```

---

#### 3.4.1 case connector

If  $\text{state}_i$  is set to **connector** then  $\text{targetQueue}_i$  is checked. In case of an empty queue,  $\text{state}_i$  remains **connector**, otherwise the next target is extracted from the queue and saved in  $z_i$  (line 5). Then the  $i$ -th robot computes a  $\bar{C}^2$  shortest and obstacle-free path  $\gamma_i$  connecting the current robot position  $q_i$  with  $z_i$  (line 6) implementing what was previously described in the start-up procedure. Finally, the robot changes the value of  $\text{state}_i$  in order to track  $\gamma_i$ . In particular, if no 'prime traveler' is present in the group, then  $\text{state}_i$  is set to **prime-traveler** (line 8). Otherwise,  $\text{state}_i$  is set to **secondary-traveler** (line 10)<sup>4</sup>.

---

<sup>4</sup> Presence of a 'prime traveler' can be easily assessed in a distributed way by, e.g., flooding (Lim and Kim 2001) on a low frequency.



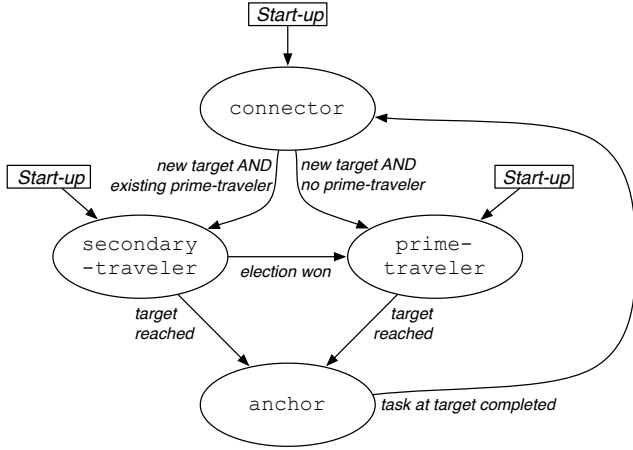


Fig. 2: State machine of the Algorithm 1.

#### 3.4.2 case *prime-traveler*

When  $\text{state}_i$  is set to **prime-traveler** (line 11) and the current position  $q_i$  is closer than  $R_z$  to the target  $z_i$  (line 12), the following actions are performed:

- the path  $\gamma_i$  is reset to **null** (line 13),
- a new distributed ‘prime traveler’ election as described in Sec. 3.3 is announced (line 14),
- the robot abdicates the role of ‘prime traveler’ and  $\text{state}_i$  is set to **anchor** (line 15).

If, otherwise,  $z_i$  is still far from the current robot position  $q_i$ , then  $\text{state}_i$  remains unchanged and the robot continues to travel towards its target.

#### 3.4.3 case *secondary-traveler*

When  $\text{state}_i$  is **secondary-traveler** (line 16) the distance  $\|q_i^\gamma - q_i\|$  to the (closest point on the) path is checked (line 17). If this distance is larger than the threshold  $R_\gamma$ , the robot replans a path from its current position  $q_i$  (line 18). This re-planning phase is necessary since a ‘secondary traveler’ could be arbitrarily far from the previously planned  $\gamma_i$  because of the ‘dragging action’ of the current ‘prime traveler’. Section 3.6 will elaborate more on this point. Subsequently, if  $q_i$  is closer than  $R_z$  to the target  $z_i$  (line 19), the path  $\gamma_i$  is reset to **null** (line 20) and  $\text{state}_i$  is set to **anchor** (line 21). Otherwise, if the target is still far away, the robot checks whether the ‘prime traveler’ abdicated and announced an election of a new ‘prime traveler’ (line 22). If this was the case, the robot takes part in the election (line 23) as described in Sec. 3.3. If the robot wins the election (line 24),  $\text{state}_i$  is set to **prime-traveler** (line 25) otherwise it remains set to **secondary-traveler**.

#### 3.4.4 case *anchor*

The last case of Algorithm 1 is when  $\text{state}_i$  is **anchor** (line 26). The robot remains in this state until the task at target  $z_i$  is completed (line 27), after which  $\text{state}_i$  is set to **connector**.

### 3.5 Completeness of the Planning Algorithm

Before illustrating the *motion control algorithm*, we state some important properties that hold during the whole execution of the planning algorithm.

**Proposition 1** *If there exists at least one target in one of the  $\text{targetQueue}_i$ , then exactly one ‘prime traveler’ will be elected at the beginning of the operation. Furthermore, this ‘prime traveler’ will keep its state until being closer than  $R_z$  to its assigned target. In the meantime no other robot can become ‘prime traveler’.*

*Proof.* The start-up procedure guarantees that, if there exists at least one target in at least one of the  $\text{targetQueue}_i$ , the group of robots includes exactly one ‘prime traveler’ and no ‘anchor’ at the beginning of the task. Any other robot is either a ‘connector’ or ‘secondary traveler’ depending on the corresponding availability of targets. During the execution of Algorithm 1, a robot can only switch into ‘prime traveler’ when being a ‘connector’ or a ‘secondary traveler’. As long as there exists a ‘prime traveler’ in the group, a ‘connector’ cannot become a ‘prime traveler’. Furthermore, a ‘secondary traveler’ becomes a ‘prime traveler’ only if it wins the election announced by the ‘prime traveler’. Since the ‘prime traveler’ allows for this election only when in the vicinity of its target (within the radius  $R_z$ ), the claim directly follows.  $\square$

Using this result, the following proposition shows that Algorithm 1 is actually guaranteed to complete the multi-target exploration in the following sense: when presented with a finite amount of targets, all targets of all robots are guaranteed to be visited in a finite amount of time. In order to show this result, an assumption on the robot motion controller is needed.

**Assumption 1.** *In a group of robots with exactly one ‘prime traveler’, the adopted motion controller is such that the ‘prime traveler’ is able to arrive closer than  $R_z$  to its target in a finite amount of time regardless of the location of the targets assigned to the other robots.*

In Sec. 3.7 we discuss in detail how the motion controller introduced in the next section 3.6 meets Assumption 1.

**Proposition 2** *Given a finite number of targets and a motion controller fulfilling Assumption 1, the whole multi-target exploration task is completed in a finite amount of time as long as the local tasks at every target can be completed in finite time.*

*Proof.* In the trivial case of no targets, the multi-target exploration task is immediately completed. Let us then assume presence of at least one target. Proposition 1 guarantees existence of exactly one ‘prime traveler’ at the beginning of the planning algorithm, and that such a ‘prime traveler’ will keep its role until reaching its target, an event that, by virtue of Assumption 1, happens in finite time. At this point, assuming as a *worst case* that no ‘secondary traveler’ has reached and cleared its own target in the meantime, one of the following situations may arise:

1. There is at least one ‘secondary traveler’. The ‘secondary traveler’ closest to its target becomes the new ‘prime traveler’ in the triggered election, and it then starts traveling towards its newly assigned target until reaching it in finite time (Proposition 1 and Assumption 1).
2. There is no ‘secondary traveler’ and no other ‘anchor’ besides the former ‘prime traveler’. In this case, no other robot has targets in its queue as, otherwise, at least one ‘secondary traveler’ would exist. Therefore, after completing its task at the target location (a finite duration), the former ‘prime traveler’ and now ‘anchor’ becomes ‘connector’ and, in case of additional targets present for this robot, it switches back into being a ‘prime traveler’ and travels towards the new targets in a finite amount of time as in case 1.
3. There is no ‘secondary traveler’, but at least one other ‘anchor’. This situation can be split again into two subcases:
  - (a) there exists at least one ‘anchor’ with a future target in its queue. Then, after a finite time, this ‘anchor’ becomes ‘secondary traveler’ and case 1 holds;
  - (b) there is no ‘anchor’ with a future target in its queue. Then, after a finite time, all ‘anchors’ have completed their local tasks and case 2 holds.

In all cases, therefore, one target is visited in finite time by the current ‘prime traveler’. Repeating this loop finitely many times, for all the (finite number of) targets, allows to conclude that *all* targets will be visited in a finite amount of time, thus showing the completeness of the planning algorithm.

If a ‘secondary traveler’ already reaches its target while the ‘prime traveler’ is active, the aforementioned worst case assumption is not valid anymore. But since,

---

#### Algorithm 2: Motion Control for Robot $i$

---

```

1 while true do
2   switch statei do
3     case connector
4       Update  $\hat{A}_p^i$  using  $\dot{\hat{A}}_p^i = k_A \sum_{j \in \mathcal{N}_i} (\hat{A}_p^j - \hat{A}_p^i)$ 
5        $f_i \leftarrow 0$ 
6     case prime-traveler
7        $\hat{A}_p^i \leftarrow \Lambda_i$  using (9)
8        $f_i \leftarrow f_{\text{travel}}(q_i, \gamma_i, v_i^{\text{cruise}})$ , using (3)
9     case secondary-traveler
10      Update  $\hat{A}_p^i$  using  $\dot{\hat{A}}_p^i = k_A \sum_{j \in \mathcal{N}_i} (\hat{A}_p^j - \hat{A}_p^i)$ 
11       $f_i \leftarrow \rho_i f_{\text{travel}}(q_i, \gamma_i, v_i^{\text{cruise}})$ , using (3) and (15)
12     case anchor
13      Update  $\hat{A}_p^i$  using  $\dot{\hat{A}}_p^i = k_A \sum_{j \in \mathcal{N}_i} (\hat{A}_p^j - \hat{A}_p^i)$ 
14       $f_i \leftarrow f_{\text{anchor}}(q_i, z_i, R_z)$ , as per (5)

```

---

in this case, the target of the ‘secondary traveler’ is already cleared, the total number of iterations is even smaller than in the previous worst case, thus still resulting in a finite completion time.  $\square$

### 3.6 Motion Control Algorithm

With reference to Algorithm 2, we now describe the motion control algorithm that runs in parallel to the planning algorithm on the  $i$ -th robot, and whose goal is to determine a traveling force  $f_i$  that can meet Assumption 1. The algorithm consists of a continuous loop, as before, in which the force  $f_i$  is computed according to the behavior encoded in the variable  $\text{state}_i$  determined by Algorithm 1:

#### 3.6.1 case *connector*

If  $\text{state}_i$  is set to **connector**, the estimate  $\hat{A}_p^i$  of the traveling efficiency of the current ‘prime traveler’ is updated with a consensus-like algorithm (line 4) that will be described in the next Sec. 3.7. The traveling force  $f_i$  is in this case simply set to 0 (line 5). It is worth mentioning that  $f_i = 0$  does not mean the  $i$ -th robot will not move, since a ‘connector’ is still dragged by the other travelers via the generalized connectivity force (according to (1), the ‘connectors’ are still subject to  $f_i^A$  and  $f_i^B$ ).

#### 3.6.2 case *prime-traveler*

If  $\text{state}_i$  is set to **prime-traveler**, the estimate  $\hat{A}_p^i$  is set to the true traveling efficiency  $\Lambda_i$ , defined by (9)

(line 7). Afterwards (line 8) the robot sets

$$f_i = f_{\text{travel}}(q_i, \gamma_i, v_i^{\text{cruise}}), \quad (2)$$

where  $f_{\text{travel}}(q_i, \gamma_i, v_i^{\text{cruise}}) \in \mathbb{R}^3$  is a proportional, derivative and feedforward controller meant to travel along  $\gamma_i$  at a given cruise speed  $v_i^{\text{cruise}}$ :

$$\begin{aligned} f_{\text{travel}}(q_i, \gamma_i, v_i^{\text{cruise}}) = & a_i^\gamma(v_i^{\text{cruise}}, q_i^\gamma) \\ & + k_v(v_i^\gamma(v_i^{\text{cruise}}, q_i^\gamma) - \dot{q}_i) \\ & + k_p(q_i^\gamma - q_i). \end{aligned} \quad (3)$$

Here,  $k_p$  and  $k_v$  are positive gains,  $q_i^\gamma$  is the point on  $\gamma_i$  closest to  $q_i$  (see Fig. 1),  $v_i^\gamma(v_i^{\text{cruise}}, q_i^\gamma)$  is the velocity vector of a virtual point traveling along  $\gamma_i$  and passing at  $q_i^\gamma$  with tangential speed  $v_i^{\text{cruise}}$ , and  $a_i^\gamma(v_i^{\text{cruise}}, q_i^\gamma)$  is the acceleration vector of the same point. It is straightforward to analytically compute both the velocity and the acceleration from  $v_i^{\text{cruise}}$ , given the spline representation of the curve (Biagiotti and Melchiorri 2008).

### 3.6.3 case *secondary-traveler*

If  $\text{state}_i$  is set to **secondary-traveler**, the estimate  $\hat{A}_p^i$  is updated with a consensus-like protocol (line 10). Then (line 11) the robot sets

$$f_i = \rho_i f_{\text{travel}}(q_i, \gamma_i, v_i^{\text{cruise}}), \quad (4)$$

where  $f_{\text{travel}}$  is defined as in (3) and  $\rho_i \in [0, 1]$  is an adaptive gain meant to scale down the intensity of the action of  $f_{\text{travel}}(q_i, \gamma_i, v_i^{\text{cruise}})$  whenever

### 3.6.4 case *anchor*

If  $\text{state}_i$  is set to **anchor**, the estimate  $\hat{A}_p^i$  is again updated using a consensus-like protocol (line 13). Then (line 14) the force  $f_i$  is set as

$$f_i = f_{\text{anchor}}(q_i, z_i, R_z) = -\frac{\partial V_{\text{anchor}}^{R_z}(\|q_i - z_i\|)}{\partial q_i} \quad (5)$$

where  $V_{\text{anchor}}^{R_z} : [0, R_z] \rightarrow [0, \infty)$  is a monotonically increasing potential function of the distance  $\ell_i = \|q_i - z_i\|$  between the robot position  $q_i$  and the target  $z_i$ , and such that  $V_{\text{anchor}}^{R_z}(0) = 0$  and  $\lim_{\ell_i \nearrow R_z} V_{\text{anchor}}^{R_z}(\ell_i) = \infty$ . Under the action of  $f_{\text{anchor}}(q_i, z_i, R_z)$  the position  $q_i$  is then guaranteed to remain confined within a sphere of radius  $R_z$  centered at  $z_i$  until the local task at the target location is completed. In our simulations and experiments we employed

$$V_{\text{anchor}}^{R_z}(\ell_i) = -k_z \frac{2R_z}{\pi} \ln \left( \cos \left( \frac{\ell_i \pi}{2R_z} \right) \right) \quad (6)$$

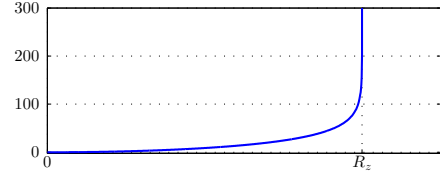


Fig. 3: Shape of the function  $V_{\text{anchor}}^{R_z}(\ell_i)$  defined in (6) that is 0 on the target  $z_i$  itself ( $\ell_i = 0$ ) and grows unbounded at the border of a sphere with radius  $R_z$ .

where  $k_z$  is an arbitrary positive constant. The shape of this function is shown in Fig. 3 and the associated  $f_{\text{anchor}}$  is

$$f_{\text{anchor}}(q_i, z_i, R_z) = -k_z \tan \left( \frac{\ell_i \pi}{2R_z} \right) \frac{q_i - z_i}{\ell_i}. \quad (7)$$

## 3.7 Traveling Efficiency, Force Alignment and Adaptive Gain

In order to implement the desired behavior we introduce two functions:

$$\Theta : \mathbb{R}^3 \times \mathbb{R}^3 \rightarrow [0, 1]$$

$$\Lambda : \mathbb{R}_0^+ \times K^* \rightarrow [0, 1]$$

where  $K^* = \{(x_c, x_M) \in \mathbb{R}^2 \mid 0 \leq x_c < x_M\}$ , defined as:

$$\Theta(x, y) = \begin{cases} \frac{1}{2} \left( 1 + \frac{x^T y}{\|x\| \|y\|} \right) & x \neq 0, y \neq 0 \\ 1 & \text{otherwise} \end{cases} \quad (8)$$

$$\Lambda(x, x_c, x_M) = \begin{cases} 1 & x \in [0, x_c] \\ \frac{1}{2} + \frac{\cos \left( \frac{x - x_c}{x_M - x_c} \pi \right)}{2} & x \in (x_c, x_M) \\ 0 & x \in [x_M, \infty). \end{cases} \quad (9)$$

Function  $\Theta(x, y)$  represents a ‘measure’ of the direction alignment of the two non-zero 3D vectors  $x$  and  $y$ . In particular,  $\Theta(x, y)$  is 1 if  $x$  and  $y$  are parallel with the same direction,  $\frac{1}{2}$  if they are orthogonal, and 0 if they are parallel with opposite direction. Note that  $\Theta(x, y)$  is equivalent to  $\frac{1}{2}(1 + \cos \theta)$  with  $\theta$  being the angle between vectors  $x$  and  $y$ .

Function  $\Lambda(x, x_c, x_M)$  ‘measures’ how small  $x$  is. If  $x \leq x_c$  then  $x$  is considered ‘small enough’ and, therefore,  $\Lambda = 1$ . If  $x \in (x_c, x_M)$  then  $\Lambda$  strictly monotonically varies from 1 to 0. If  $x \geq x_M$ , then  $\Lambda = 0$ . The shape of  $\Lambda$  is depicted in Fig. 4.

Having introduced these functions, we now define the *force direction alignment* of the  $i$ -th robot as

$$\Theta_i = \Theta(f_i^\lambda, f_{\text{travel}}(q_i, \gamma_i, v_i^{\text{cruise}})), \quad (10)$$

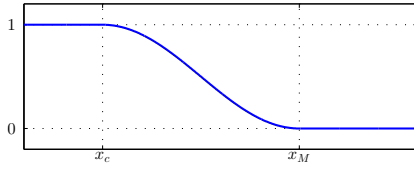


Fig. 4: Sketch of the function  $\Lambda(x, x_c, x_M)$  for fixed  $x_c$  and  $x_M$ .

and note that  $\Theta_i$  can be locally computed by the  $i$ -th robot. The quantity  $\Theta_i$  thus represents an index in  $[0, 1]$  measuring the degree of conflict among the directions of the generalized connectivity force and the traveling force.

When  $\gamma_i \neq \text{null}$ , we also define the absolute tracking error as

$$e_i = (1 - \alpha_A) \|v_i^\gamma(v_i^{\text{cruise}}, q_i^\gamma) - \dot{q}_i\| + \alpha_A \|q_i^\gamma - q_i\|, \quad (11)$$

with  $\alpha_A \in [0, 1]$  being a constant parameter modulating the importance of the velocity tracking error w.r.t. the position tracking error. The *traveling efficiency* is then defined as

$$\Lambda_i = \Lambda(e_i, x_c, x_M), \quad (12)$$

where  $0 \leq x_c < x_M < \infty$  are two user-defined thresholds representing the point at which the traveling efficiency  $\Lambda_i$  starts to decrease and the maximum tolerated error after which the traveling efficiency vanishes. In this way it is possible to evaluate how well a traveler can follow its desired planned path according to a suitable combination of velocity and position accuracy. It is important to note that the value  $\Lambda_i = 1$  does not imply an exact tracking of the path, but it still allows a small tracking tolerance (dependent on the parameter  $x_c$ ). Similarly, the value  $\Lambda_i = 0$  does not imply a complete loss of path tracking, but it represents the possibility of a tracking error higher than a maximum threshold (dependent on  $x_M$ ).

In order to meet Assumption 1, we are only interested in the traveling efficiency of the current ‘prime traveler’ for monitoring whether (and how much) its exploration task is held back by the presence/motion of the ‘secondary travelers’. From now on we then denote this value as  $\Lambda_p$ , where

$$p = i \quad \text{s.t.} \quad \text{state}_i = \text{prime-traveler}.$$

This quantity is not in general locally available to every robot in the group, and therefore a simple decentralized algorithm is used for its propagation to avoid a flooding step. Among many possible choices we opted

for using the following well-known consensus-based propagation (Olfati-Saber and Murray 2003):

$$\begin{aligned} \dot{\hat{\Lambda}}_p^i &= k_A \sum_{j \in \mathcal{N}_i} (\hat{\Lambda}_p^j - \hat{\Lambda}_p^i) & \text{if } i \neq p \\ \hat{\Lambda}_p^i &= \Lambda_i & \text{if } i = p. \end{aligned} \quad (13)$$

This distributed estimator lets  $\hat{\Lambda}_p^i$  track  $\Lambda_p$  for all  $i$  that hold  $\text{state}_i \neq \text{prime-traveler}$  with an accuracy depending on the chosen gain  $k_A$ . Notice that, for a constant  $\Lambda_p$ , the convergence of this estimation scheme is exact. Furthermore, since  $\Lambda_p \in [0, 1]$ ,  $\hat{\Lambda}_p^i$  is then saturated so as to remain in the allowed interval despite the possible transient oscillations of the estimator. Instead of this simple consensus, one could also resort to a PI average consensus estimator (Freeman et al. 2006) to cope with presence of a time-varying signal. However, for simplicity we relied on a simple consensus law with less parameters to be tuned, and with, nevertheless, a satisfying performance as extensively shown in our simulation and experimental results.

Hence, every ‘secondary traveler’ can locally compute  $\Theta_i$  and build an estimation  $\hat{\Lambda}_p^i$  of  $\Lambda_p$ . In order to consolidate these two quantities into a single value, we define the function  $\rho : [0, 1] \times [0, 1] \times [1, \infty) \rightarrow [0, 1]$  as:

$$\rho(x, y, \sigma) = (1 - x)y^\sigma + x(1 - (1 - y)^\sigma), \quad (14)$$

where  $1 \leq \sigma < \infty$  is a constant parameter. Gain  $\rho_i$  is then obtained from  $\Theta_i$  and  $\hat{\Lambda}_p^i$  as

$$\rho_i = \rho(\Theta_i, \hat{\Lambda}_p^i, \sigma) \quad (15)$$

with  $1 \leq \sigma < \infty$  being a tunable parameter.

The reasons motivating this design of gain  $\rho_i$  are as follows:  $\rho_i$  is a smooth function of  $\Theta_i$  and  $\hat{\Lambda}_p^i$  possessing the following desired properties (see also Fig. 5)

1.  $\hat{\Lambda}_p^i = 1 \Rightarrow \rho_i = 1$ : if the traveling efficiency of the ‘prime traveler’ is 1 then every ‘secondary traveler’ sets  $f_i = f_{\text{travel}}(q_i, \gamma_i, v_i^{\text{cruise}})$ ;
2.  $\hat{\Lambda}_p^i = 0 \Rightarrow \rho_i = 0$ : if the traveling efficiency of the ‘prime traveler’ is 0 then every ‘secondary traveler’ sets  $f_i = 0$ ;
3.  $\rho_i$  monotonically increases w.r.t.  $\hat{\Lambda}_p^i$  for any  $\Theta_i$  and  $\sigma$  in their domains;
4.  $\rho_i$  constantly increases w.r.t.  $\Theta_i$  for any  $\hat{\Lambda}_p^i \in (0, 1)$  and  $\sigma > 1$ ;
5. if  $\sigma = 1$  then  $\rho_i = \hat{\Lambda}_p^i$  for any  $\Theta_i \in [0, 1]$ ;
6. if  $\sigma \rightarrow \infty$  then  $\rho_i \rightarrow \Theta_i$  for any  $\hat{\Lambda}_p^i \in (0, 1)$ .

Summarizing, gain  $\rho_i$  mixes the information of both the force direction alignment and the traveling efficiency of the ‘prime traveler’, with more emphasis on the first or the second term depending on the value of the parameter  $\sigma$ . Nevertheless, the traveling efficiency  $\hat{\Lambda}_p^i$  is

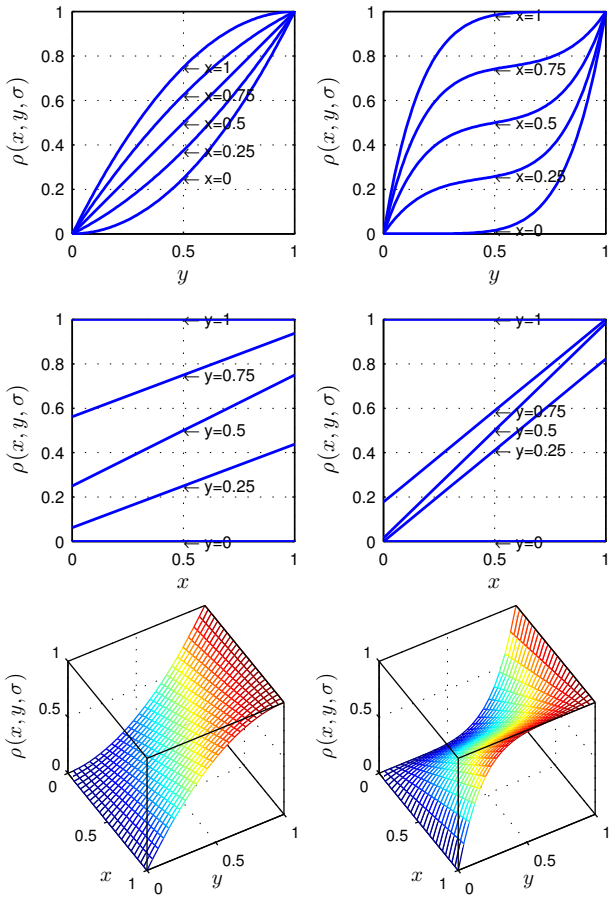


Fig. 5: Function  $\rho$  for  $\sigma = 2$  (left side) and  $\sigma = 6$  (right side). The motion controller exploits this function by plugging the force direction alignment in the  $x$  argument, and the estimate of the traveling efficiency of the current ‘prime traveler’ in the  $y$  argument.

always predominant at its boundary values (0 and 1) regardless of the value of  $\sigma$ . This means that, whenever the estimated travel efficiency of the ‘prime traveler’ is  $\hat{A}_p^i = 0$  and robot  $i$  is a ‘secondary traveler’, its traveling force is scaled to zero and, therefore, robot  $i$  only becomes subject to the connectivity and damping force. Therefore, in this situation the motion of all ‘secondary travelers’ results dominated by the ‘prime traveler’, which is then able to execute its planned path towards its target location. On the other hand, when  $\hat{A}_p^i = 1$ , the ‘prime traveler’ has a sufficiently high traveling efficiency despite the ‘secondary traveler’ motions. Therefore, every ‘secondary traveler’ is free to travel along its own planned path regardless of the direction alignment between traveling and connectivity force.

We conclude noting that the main goal of the machinery defined in Sec. 3.6–Sec. 3.7 is to ensure that the motion controller meets the requirements defined in Assumption 1. Although some of the steps involved

in the design of the traveling force  $f_i$  have a ‘heuristic’ nature, the proposed algorithm is quite effective in solving the multi-target exploration task (in a decentralized way) under the constraint of connectivity maintenance, as proven by the several simulation and experimental results reported in the next section.

## 4 Simulations and experiments

In this section, we report the results of an extensive simulative and experimental campaign meant to illustrate and validate the proposed method. The videos of the simulations and experiments can be watched in the attached material and on [http://homepages.laas.fr/afranchi/videos/multi\\_exp\\_conn.html](http://homepages.laas.fr/afranchi/videos/multi_exp_conn.html).

All the simulation (and experimental) results were run in 3D environments, although only a 2D perspective is reported in the videos for the simulated cases (therefore, robots that may look as ‘colliding’ are actually flying at different heights, since their generalized connectivity force prevents any possible inter-robot collision).

As robotic platform in both simulations and experiments we used small quadrotor UAVs (Unmanned Aerial Vehicles) with a diameter of 0.5 m. This choice is motivated by the versatility and construction simplicity of these platforms, and also because of the good match with our assumption of being able to track any sufficiently smooth linear trajectory in 3D space.

We further made use of the SwarmSimX environment (Lächele et al. 2012), a physically-realistic simulation software. The simulated quadrotors are highly detailed models of the real quadrotors later employed in the experiments. The physical behavior of the robots itself and their interaction with the environment is simulated in real-time using PhysX<sup>5</sup>.

For the experiments, we opted for a highly customized version of the MK-Quadro<sup>6</sup>. We implemented a software on the onboard microcontroller able to control the orientation of the robot by relying on the integrated inertial measurement unit. The desired orientation is provided via a serial connection by a position controller implemented within the ROS framework<sup>7</sup> that can run on any generic GNU-Linux machine. The machine can be either mounted onboard or acting as a base-station. In the latter case a wireless serial connection with XBees<sup>8</sup> is used. We opted for the separate base station in order to extend the flight time thanks

<sup>5</sup> <http://www.geforce.com/hardware/technology/physx>

<sup>6</sup> <http://www.mikrokoetter.com>

<sup>7</sup> <http://www.ros.org>

<sup>8</sup> <http://www.digi.com/lp/xbee>

to the reduction of the onboard weight. The current UAV position used by the controller is retrieved from a motion capturing system<sup>9</sup>, while obstacles are defined statically before the task execution.

To abstract from simulations and experiments, we used the TeleKyb software framework, which is thoroughly described in Grabe et al. (2013). Finally, the desired trajectory (consisting of position, velocity and acceleration) is generated by our decentralized control algorithm implemented using Simulink<sup>10</sup> running in real-time at 1 kHz.

#### 4.1 Monte Carlo Simulations

The proposed method has been extensively evaluated through randomized experiments in three significantly different scenarios. The first scenario is an obstacle free 3D space and three snapshots of the evolution of the proposed algorithm are presented in Fig. 6. The second, a more complex, scenario includes a part of a town and is reported in Fig. 7. The third is an office-like environment shown in Fig. 8. The size of the environments is 50 m × 70 m for both the empty space and the town, and about 10 m × 15 m for the office. Since the first two environments are outdoor scenarios and the office-like environment is indoor, two different sets of parameters were employed in the simulations and which are listed. The values of the main parameters are listed in Table 2.

Table 2: Main parameters of the algorithm used in the 1800 randomized simulative trials in the different scenarios.

parameter	empty space and town	office
$(R'_s, R_s)$	(2.5 m, 6 m)	(1.1 m, 2.5 m)
$(R'_o, R'_o)$	(0.75 m, 1.75 m)	(0.25 m, 0.6 m)
$(R'_c, R'_c)$	(1 m, 2.5 m)	(0.8 m, 1.1 m)
$(\lambda_2^{\min}, \lambda_2^{\text{null}})$	(0, 1)	(0, 1)
$\sigma$	0.75 m	0.25 m
$v_i^{\text{cruise}}$	3	3
$(x_c, x_M)$	3 m/s	1 m/s for all $i$
$\Delta t_i^k$	(0.1, 0.6) $v_i^{\text{cruise}}$	(0.1, 0.6) $v_i^{\text{cruise}}$
$R_z$	3 s for all $i$ and $k$	3 s for all $i$ and $k$
	1.8 m	1 m

The number of robots varied from 10 to 35. In every trial 3 targets are sequentially assigned to 5 robots and 2 targets are sequentially assigned to other 5 robots, for a total of 25 targets per trial. The remaining robots are given no targets (i.e., they act always as ‘connectors’).

The configuration of the given targets is randomized across the different trials. The same random configurations are repeated for every different number of robots

in order to allow for a fair comparison among the results. In the following we refer to the robots with at least one target assigned during a trial as ‘explorers’.

To summarize, we simulated a total number of 1800 trials arranged in the following way: in each of the 3 scenes, and for each of the 100 target configurations in each scene, we ran a simulation with 6 different numbers of robots, namely 10, 15, 20, 25, 30, 35. We encourage the reader to also watch the attached video where some representative simulative trials are shown.

In Fig. 9 we show the evolutions of the statistical percentiles of:

- the overall completion time,
- the mean traveled distance of the 10 ‘explorers’,
- the maximum Euclidean distance between two ‘explorers’
- the average of  $\lambda_2(t)$  over time along the whole trial (we recall that the larger the  $\lambda_2$  the more connected is the group of robots, refer to Appendix A),

when the number of robots varies from 10 (i.e., no ‘connectors’) to 35 (i.e., 25 ‘connectors’). Each column refers to one of the 3 different scenarios.

An improvement with the increasing number of ‘connectors’ in all scenarios is obvious. The mean completion time (first row) roughly halves when comparing 0 to 25 ‘connectors’.

In the second row (mean traveled distance) one can see how, by already adding a few robots, a reduced mean traveled distance is obtained. This can be explained by the fact that the ‘connectors’ make the ‘explorers’ less disturbed by other ‘explorers’ with, therefore, more freedom to avoid unnecessary detours in reaching their targets.

Another measure of the reduced task completion time is the maximum stretch among the ‘explorers’ (i.e., the maximum Euclidean distance between any two ‘explorers’, see third row). The more connectors, the more stretch is allowed: ‘connectors’ in fact provide the support needed by the ‘explorers’ for keeping graph  $\mathcal{G}$  connected while freely moving towards their targets. Only the office-like environment does not show this trend in the maximum stretch. This is due to the fact that the scene is relatively small and therefore the targets are not enough spread apart, so no bigger stretch is needed.

The increased freedom of the ‘explorers’ is also evident in the plots of the average  $\lambda_2(t)$  (fourth row). These plots show how the ‘connectors’ are also useful to let the ‘explorers’ move more freely even in small environments. In fact, the larger the amount of ‘connectors’, the lower the mean  $\lambda_2$ : with more connectors the ‘explorers’ are more able to simultaneously travel towards their targets, thus bringing the topology of the

<sup>9</sup> <http://www.vicon.com>

<sup>10</sup> <http://www.mathworks.com/products/simulink/>

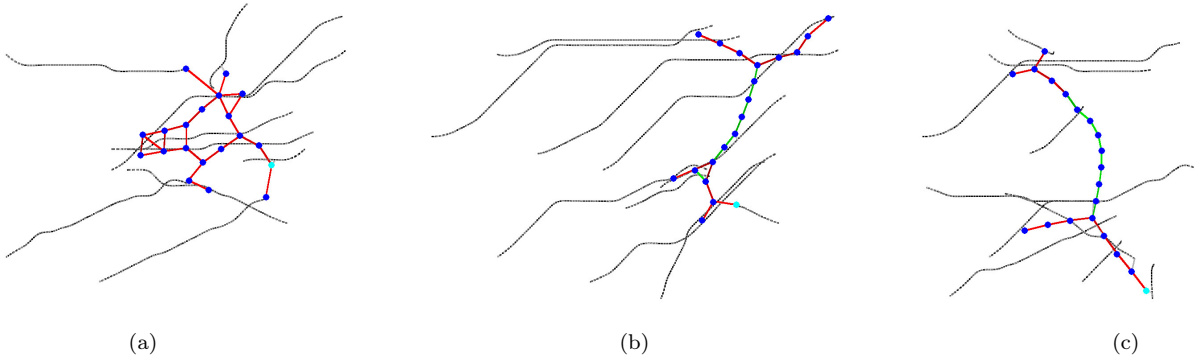


Fig. 6: Snapshots of a simulation with 20 UAVs in empty space in three different consecutive time instants. The dotted black curves represent the planned path  $\gamma_i$  to the current target for each robot  $i$  (if it has a current target). Blue dots are the robots, the turquoise dot is the current ‘prime traveler’. Line segments represent the presence of a connection link between a pair of robots with the following color coding: green – well connected, red – close to disconnection. The robots are able to concurrently explore the given targets and continuously maintain the connectivity of the interaction graph.

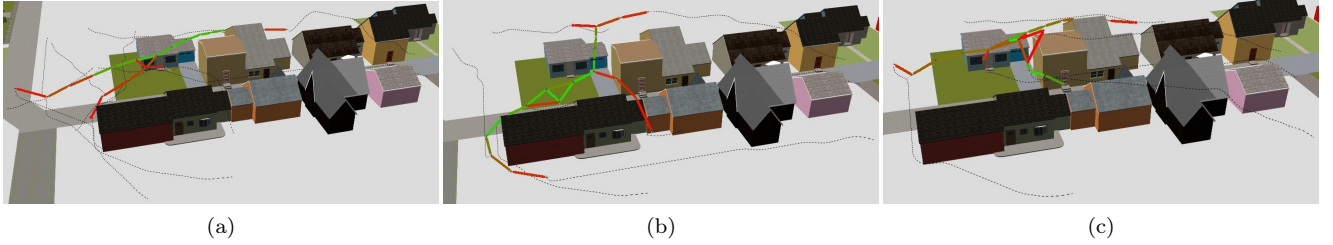


Fig. 7: Three snapshots of consecutive time instants of a simulation in the town environment. Graphical notation similar to Fig. 6

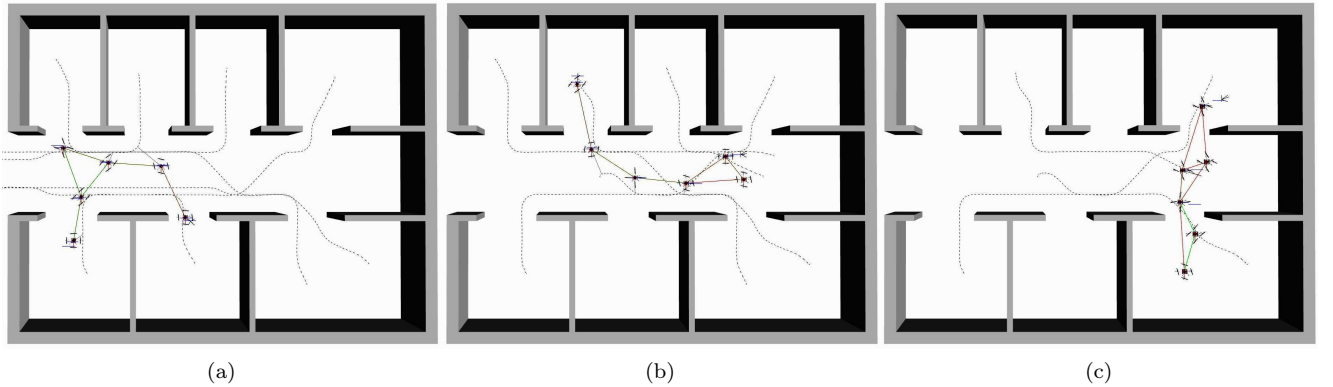


Fig. 8: Snapshots of a simulation in the office-like environment in three consecutive time instants. Graphical notation similar to Fig. 6

group closer to less connected topologies (i.e., closer to tree-like topologies where the explorers would be the leaves of the tree). Clearly, this effect is independent of the maximum stretch, in fact the average  $\lambda_2$  follows this decreasing trend also in the third office-like environment (third column).

## 4.2 Experiments

The experiments involved 6 real quadrotors and were meant to test the applicability of the algorithm in a real scenario. The parameters of the algorithm used in the experiments are reported in Table 3.

For these experiments, we reproduced a scene similar to the office-like environment used in simulation, see Fig. 12. The UAVs with IDs ‘2’ and ‘4’ (called ‘explorers’) were given some targets, while the UAVs with



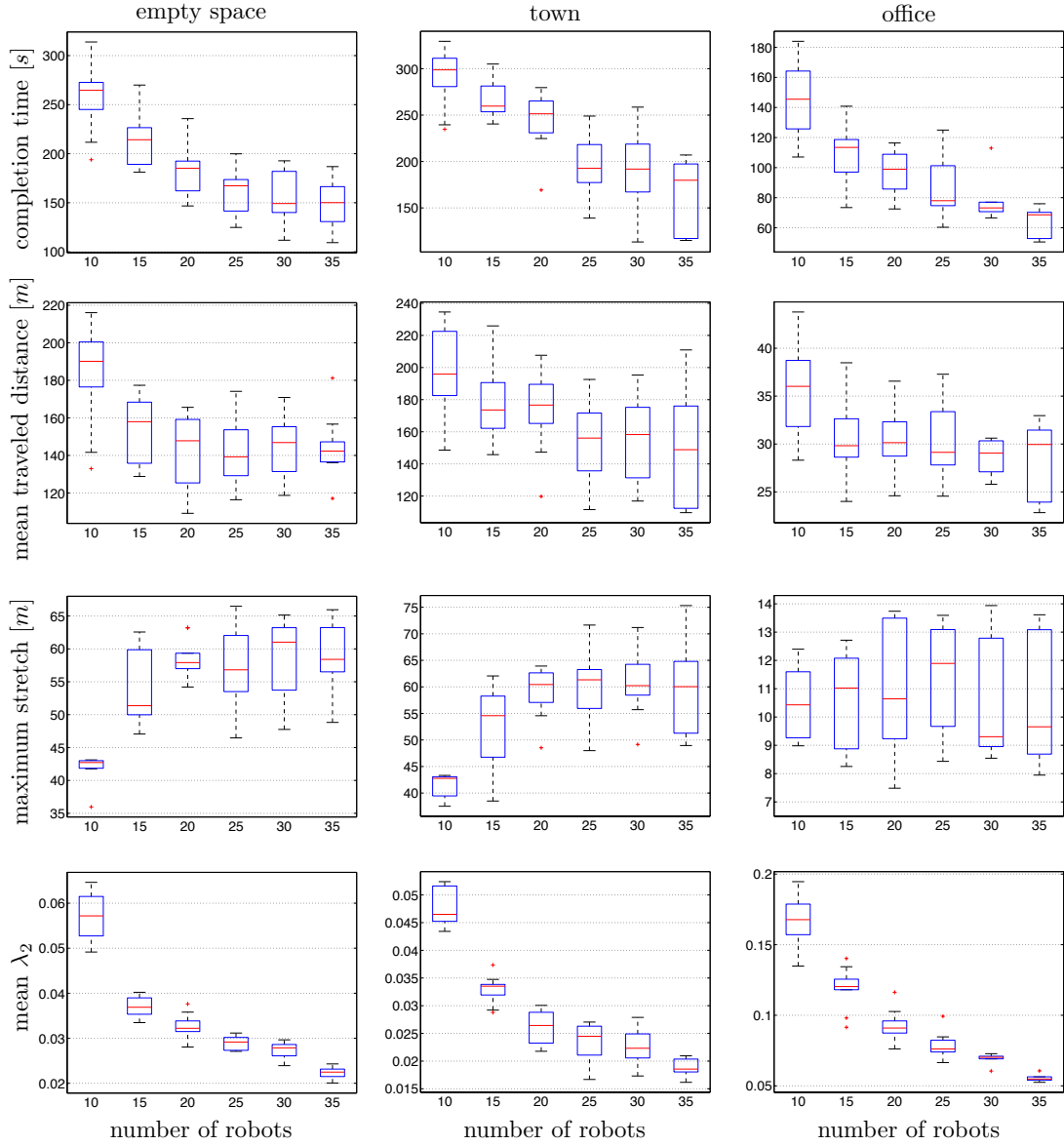


Fig. 9: Statistics of the completion times (first row), mean traveled distance of the traveling robots (second row), the maximum Euclidian distance between two traveling robots (third row) and mean  $\lambda_2$  (forth row) versus the number of robots in the environments empty space (left column), town (middle column) and office (right column).

IDs ‘1’, ‘3’, ‘5’, and ‘6’ (‘connectors’) had no target, for then a total of 6 quadrotors.

The ‘explorer’ 1 (with ID ‘4’) carries an onboard camera and has two targets in total. Whenever it reaches one of its targets it gives a human operator direct control of the vehicle in the surrounding area of the target. Then, with the help of the onboard camera, the human operator has the task of searching for an object in the environment. When the object is found by the human operator, the task at the target is considered completed, and the UAV switches back to autonomous control. In order to allow full human control of ‘explorer’ 1 in the anchoring behavior, the UAV is temporarily decoupled

from the point  $q_4$ , which is instead kept close to the target by the action of  $f_{\text{anchor}}$  (as desired). The ‘explorer’ 2 (with ID ‘2’) is instead fully autonomous and is assigned with a total of 4 targets. At the first target location, the task is to pick up an object to then be released at the second target location. The same task is subsequently repeated with targets 3 and 4. We note, however, that the pick and place action is only virtually performed since the employed quadrotors are not equipped with an onboard gripper. We also stress that all these operations are performed concurrently while keeping the topology of the group connected at all times.



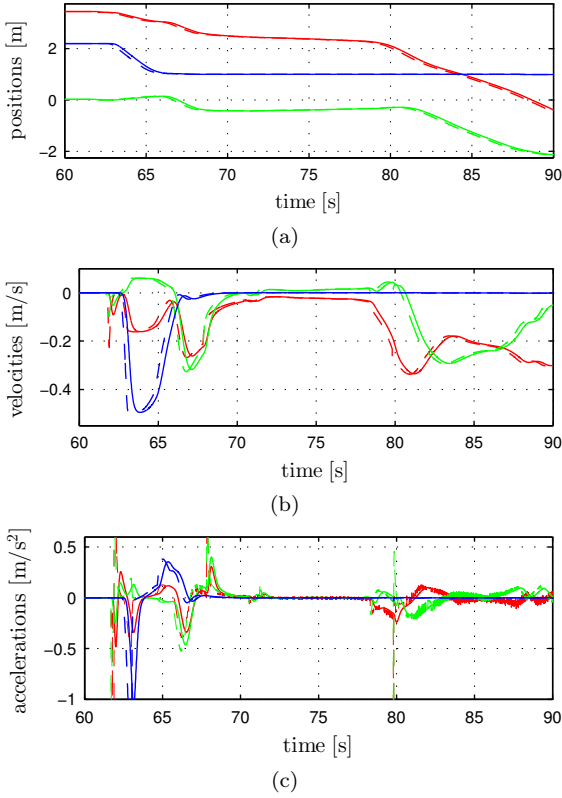


Fig. 10: Position, velocity and acceleration of ‘explorer’ 1 during a representative period of the experiment, where  $q_i(t)$ ,  $\dot{q}_i(t)$ ,  $\ddot{q}_i(t)$  are plotted in dash and  $q_i^f(t)$ ,  $\dot{q}_i^f(t)$ ,  $\ddot{q}_i^f(t)$  as solid curves. The  $x$ ,  $y$  and  $z$  component is plotted in red, green and blue respectively.

A video of the experiment is present in the attached material and can be found under the given link above.

Table 4 reports and describes all the relevant events taking place during an experiment in a chronological order.

Figure 12 shows the top-view of the ‘explorer’ paths for five representative time periods:  $T_1 = [0, 25]$  s in Fig. 12a,  $T_2 = [25, 60]$  s in Fig. 12b,  $T_3 = [60, 80]$  s in Fig. 12c,  $T_4 = [80, 120]$  s in Fig. 12d, and finally  $T_5 = [120, 129]$  s in Fig. 12e. Every plot shows the (connected) graph topology of the group at the beginning

Table 3: Main parameters used in the experiments.

parameter	value
$(R'_s, R_s)$	(1.4 m, 2.5 m)
$(R_o, R'_o)$	(0.5 m, 0.75 m)
$(R_c, R'_c)$	(1.0 m, 1.4 m)
$(\lambda_2^{\min}, \lambda_2^{\text{null}})$	(0, 1)
$R_{\text{grid}}$	0.2 m
$\sigma$	3
$v_i^{\text{cruise}}$	0.5 m/s
$(x_c, x_M)$	$(0.2, 0.7) v_i^{\text{cruise}}$
$\Delta t_i^k$	3 s for all $i$ and $k$
$R_z$	0.75 m

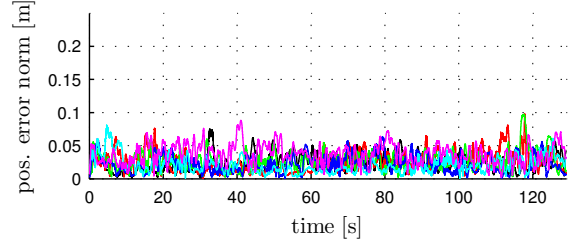


Fig. 11: Plots of the 6 norms of the position error between  $q_i(t)$  and the corresponding real quadrotor trajectory, for  $i = 1, \dots, 6$ . The average error norm is 0.021 m.

of the time interval (dashed black lines) and the paths of the 2 ‘explorers’ (solid lines, blue for the ‘explorer’ 1 and red for the ‘explorer’ 2). The initial positions of the robots are shown with colored circles and are labeled with the IDs of the corresponding robots. The two small blue squares represent the two desired target locations of the ‘explorer’ 1. The two green squares and the two red squares represent the two pick positions and release positions of ‘explorer’ 2, respectively. Finally, the vertical walls of the environment are shown in gray. Figure 12f on the other hand shows the  $z$ -coordinate of all the six quadrotors in order to understand the 3D motion in the 2D projections of Figs. 12a to 12e.

Figure 13 shows three screenshots of the experiment: the lines between two quadrotors represent the corresponding connecting link as per graph  $\mathcal{G}$ .

Finally, Fig. 14 reports nine plots that capture the behavior of several quantities of interest throughout the whole experiment. As can be seen in Fig. 14a, the generalized algebraic connectivity eigenvalue  $\lambda_2(t)$  (see Appendix A) remains positive for any  $t > 0$ , thus implying continuous connectivity of the graph  $\mathcal{G}$  as desired. The time-varying number of edges in Fig. 14b shows the dynamic reconfiguration of the group topology which ranges between topologies with 5 edges (the minimum for having  $\mathcal{G}$  connected) and topologies with up to 10 edges. This plot clearly shows how the adopted connectivity maintenance approach can cope with time-varying graphs. In Fig. 14c, we report the stretch of the group, defined as the maximum Euclidean distance between any two robots at a given time  $t$ . One can then appreciate how this stretch varies among 3.5 and 7.5 meters thus exploiting at most the allowable ranges of the experimental arena. Notice also how the stretch is in general larger when the number of links (and consequently  $\lambda_2(t)$ ) is smaller. In fact the two peaks at about 60 s and 103 s occur when the robots are forced into a sparsely connected topology because the two ‘explorers’ have concurrently reached their farthest target pairs, i.e.,  $(A_1, B_2)$  and  $(B_1, D_2)$ .

Table 4: Chronological list of important events in the experiment.

Fig. 12	Time	Events
Fig. 12a	0 s	The experiment starts. Both ‘explorers’ are assigned a target and since ‘explorer’ 2 is closer to its goal, it becomes ‘prime traveler’, while ‘explorer’ 1 is ‘secondary traveler’.
	22 s	‘Explorer’ 2 arrives at its first target, where it should pick up an object. Therefore ‘explorer’ 2 goes into ‘anchor’ and ‘explorer’ 1 becomes ‘prime traveler’.
Fig. 12b	29 s	‘Explorer’ 2 has completed the pick-up action and receives the point to release the object as a new target. Since ‘explorer’ 1 is still ‘prime traveler’, ‘explorer’ 2 becomes ‘secondary traveler’.
	35 s	‘Explorer’ 1 arrives at its target, where the human operator takes control of the UAV and use its camera to find a yellow picture on the wall. ‘Explorer’ 2 then becomes ‘prime traveler’.
	56 s	‘Explorer’ 2 arrives at the target where it needs to release the object.
Fig. 12c	63 s	‘Explorer’ 2 has completed the releasing action and receives the next pick-up location. ‘Explorer’ 1 is still under the control of the human operator and therefore in an ‘anchor’ state, so ‘explorer’ 2 directly becomes ‘prime traveler’.
	65 s	The human operator finds the picture on the wall, ‘explorer’ 1 becomes autonomous again and starts to move towards its next target as ‘secondary traveler’, since ‘explorer’ 2 is ‘prime traveler’.
	78 s	‘Explorer’ 2 arrives at the location where to pick up the second object and goes to the ‘anchor’ state. Hence ‘explorer’ 1 becomes ‘prime traveler’.
Fig. 12d	85 s	‘Explorer’ 2 has completed the pick-up action and starts moving towards the releasing location as ‘secondary traveler’.
	100 s	‘explorer’ 1 arrives at its target, goes to ‘anchor’ state and is thus under control of the human operator, therefore ‘explorer’ 2 becomes ‘prime traveler’.
	119 s	‘Explorer’ 2 arrives at its final target and switches into ‘anchor’.
Fig. 12e	123 s	The human operator finds the searched object and ‘explorer’ 1 becomes ‘connector’ since it has no new target location.
	126 s	‘Explorer’ 2 has completed the releasing action and becomes a ‘connector’ since it has also no new target.
	129 s	No UAV has a next target and the experiment ends.

Figure 14d shows the ‘explorer’ states  $state_2$  and  $state_4$  over time, with a dashed blue line and solid red line, respectively. In the plot, the following code is used: 1 = ‘prime traveler’, 2 = ‘secondary traveler’, 3 = ‘anchor’ and 4 = ‘connector’. For  $i = 1, 3, 5, 6$  it is  $state_i = 4$  for all  $t \in [0, 129]$ . Notice that, because of the

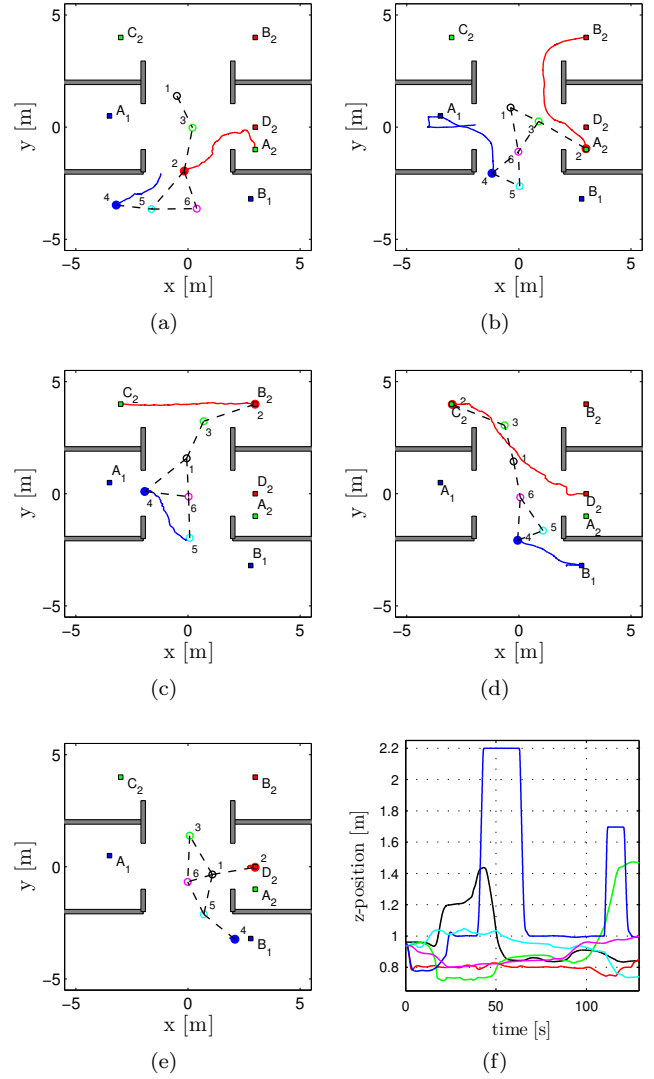


Fig. 12: (a)-(e) Top view of the 3D paths of the ‘explorers’ (solid blue and red curves) during the experiment in five representative time intervals. The interaction graph at the beginning of each interval is shown with black dashed lines. The ID of each robot is shown besides the circle representing the starting position of each robot at the beginning of the corresponding interval. Targets are represented with colored squares and walls are gray. The specific time intervals are: (a)  $T_1 = [0, 25]$  s, (b)  $T_2 = [25, 60]$  s, (c)  $T_3 = [60, 80]$  s, (d)  $T_4 = [80, 120]$  s and (e)  $T_5 = [120, 129]$  s. (f) z-coordinate of the positions of all six quadrotors to help interpreting the 2D projection reported in the plots (and videos). The large vertical motion of ‘explorer’ 1 (blue) is due to the human operator flying this robot, while the subsequent descent is autonomously performed thanks to the proposed algorithm.

algorithm design, at most one ‘explorer’ has  $state_i = 1$  at any given time.

The temporary decoupling of the ‘explorers’ from the points  $q_2$  and  $q_4$  during their anchoring behavior can be appreciated in Fig. 14e, where the Euclidian distance between the real robot position in the trajectory

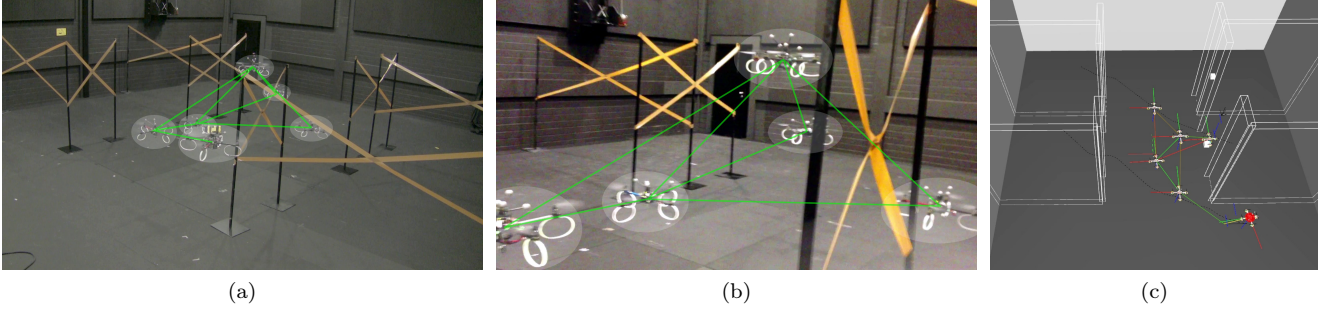


Fig. 13: Three simultaneous screenshots of the experiment described in the text: (a) shows the side view of the scene from a fixed camera. Connections between UAVs (brightened areas) are overlaid as green lines. (b) shows the view taken from the onboard camera of the ‘explorer’ 1 using the same highlighting. (c) shows a 3D synthetic reconstruction of the robot positions and connections are shown with a line given in green when the weight is high, red shortly before a connection breaks and as a gradient in between. The robot that is marked with the red sphere is currently decoupled and controlled by the human operator.

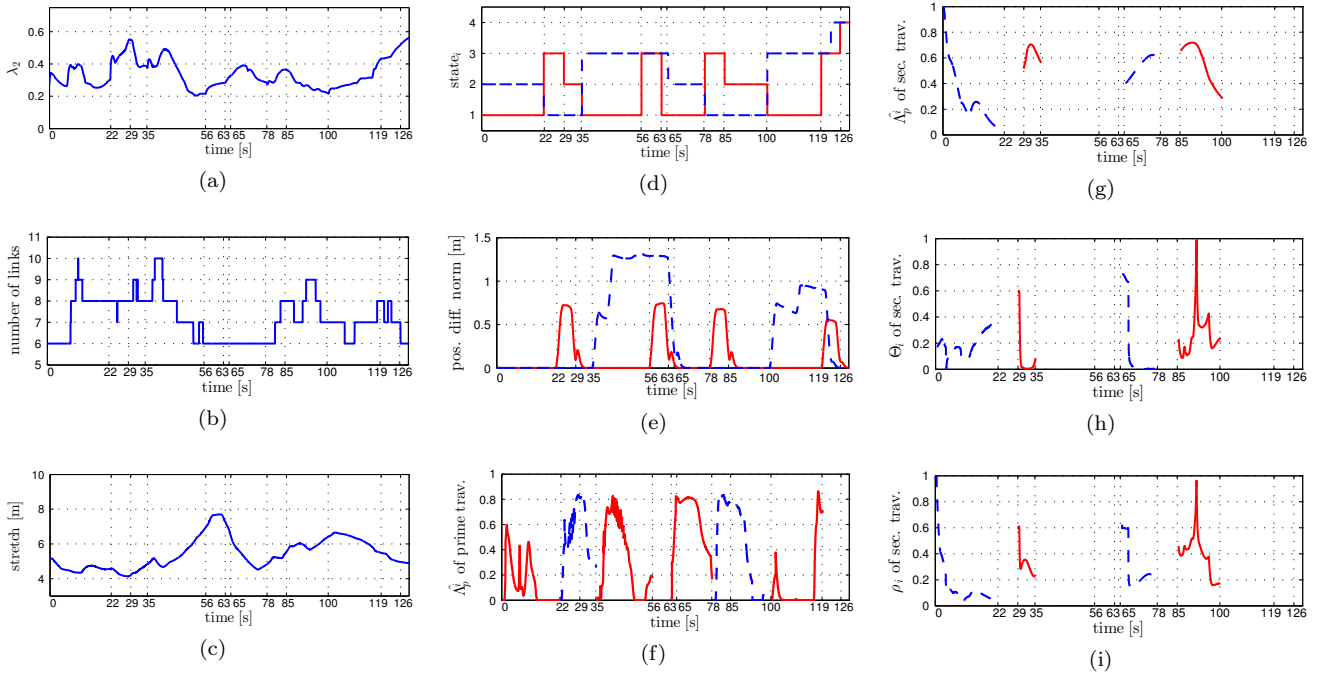


Fig. 14: Behavior of different measurements during an experiment: (a)  $\lambda_2$  always keeps greater than zero, thus showing how the group remains connected at all times, (b) the number of links  $|\mathcal{E}(t)|$  of the interaction graph  $\mathcal{G}(t)$ , (c) the stretch of the formation given by the maximum Euclidean distance between any two quadrotors over time, (d) the exploration states with the following meaning: 1: ‘prime traveler’, 2: ‘secondary traveler’, 3: ‘anchor’, 4: ‘connector’, (e) the position difference between the virtual point of the connectivity maintenance and the commanded position to the quadrotors showing the decoupling as an ‘anchor’, (f) the traveling efficiency of the current ‘prime traveler’ (see (12)), (g) the estimation of the traveling efficiency by the ‘secondary travelers’ (see (13)), (h) the force direction alignment for the ‘secondary travelers’ (see (10)), (i) the adaptive gain used by the ‘secondary travelers’ to scale down their traveling force (see (15)).

and the corresponding  $q_i(t)$  is shown, for  $i = 2, 4$ . ‘Explorer’ 1 (solid red line) decouples four times in total, in correspondence of the 2 pick-and-place operations, which gives rise to 4 short peaks in the plot. ‘Explorer’ 2 (dashed blue line) decouples two times in total, in correspondence of the 2 human-in-the-loop operations, causing 2 long peaks in the plot.

Figure 14f shows the traveling efficiency  $\lambda_p$  of the current ‘prime traveler’ with a dashed blue line when ‘explorer’ 1 is the ‘prime traveler’ and with a solid red line when ‘explorer’ 2 is the ‘prime traveler’. The estimation  $\hat{\lambda}_p^i$  of this value (see (13)) by all robots that are currently not ‘prime traveler’ is given in Fig. 15. We chose  $k_A = 1$  resulting in a relatively slow propagation to show the additional robustness of our algo-

rithm against this parameter (and the simple adopted consensus propagation), but clearly one could easily employ higher gains. To make it easier for the reader to understand the following discussion, we show again in Fig. 14g the essential information of this last plot whenever a robot is a ‘secondary traveler’. In Figs. 14h and 14i the force direction alignment  $\Theta_i$  (see (10)) and the adaptive gain  $\rho_i$  (see (15)) of the current ‘secondary traveler’ are shown. In the latter three plots a dashed blue line indicates when ‘explorer’ 1 is the ‘secondary traveler’, and a solid red line when ‘explorer’ 2 is the ‘secondary traveler’.

To fully understand the important features of our method, we now give a detailed description of the time interval  $[0, 22]$  in the Figs. 14f to 14i. A similar pattern can then be found in the rest of the experiment. In this time interval, the ‘explorer’ 2 is the ‘prime traveler’, while ‘explorer’ 1 is a ‘secondary traveler’ (and the rest are ‘connectors’). Due to the initial transient of its motion controller, the ‘prime traveler’ starts with  $A_p = 0$  and quickly reaches  $A_p = 0.6$ . Shortly after, the traveling efficiency decreases again since ‘explorer’ 2 reaches the end of the area where it can freely move and, thus, needs to ‘pull’ the other robots for preserving connectivity of  $\mathcal{G}$ . This effect is propagated to the ‘explorer’ 1 as shown in Fig. 14g. The force direction alignment between the traveling force and the generalized connectivity force is shown in Fig. 14h. Combining these two plots with (15) allows to understand the effect of Fig. 14i. As can be seen, the ‘secondary traveler’ slows down its motion to around 10% for roughly 5 seconds. This enables the ‘prime traveler’ to travel faster again (see Fig. 14f). However, since the ‘explorer’ 2 needs to move around the wall (see Fig. 12a) to reach its target, it needs to ‘pull’ the other robots even more for preserving connectivity. Therefore, the traveling efficiency becomes zero and, although the direction alignment of the ‘secondary traveler’ becomes higher, the overall gain  $\rho_i$  stays very low: this makes it possible for the ‘prime traveler’ to eventually reach its target. We recall here that, according to Table 3 and (9),  $A_p = 1$  as soon as the ‘prime traveler’ achieves a speed of at least 80% of its desired cruise speed (so the error is less than 20%), while  $A_p = 0$  means a speed of less than 30% (an error of more than 70%), and *not necessarily* a zero velocity.

## 5 Conclusions

In this paper we presented a novel distributed and decentralized control strategy that enables simultaneous multi-target exploration while ensuring a time-varying connected topology in a 3D cluttered environment. We provided a detailed description of our algorithm which

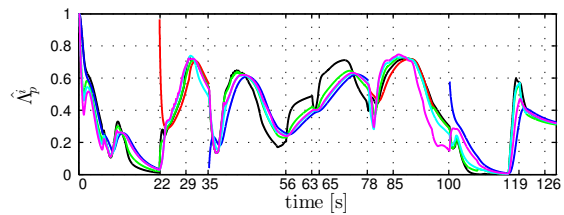


Fig. 15:

effectively exploits presence of *four* dynamic roles for the robots in the group. In particular, a ‘connector’ is a robot with no active target, an ‘anchor’ a robot close to its desired location, and all other robots are instead moving towards their targets. Presence of at most one ‘prime traveler’, holding a leader virtue, is always guaranteed. All other robots (‘secondary travelers’) are bound to adapt their motion plan so as to facilitate the ‘prime traveler’ visiting task. This feature ensures that the ‘prime traveler’ is always able to reach its target, and thus ultimately allows to conclude completeness of the exploration strategy. The scalability and effectiveness of the proposed method was shown by presenting a complete and extensive set of simulative results, as well as an experimental validation with real robots for further demonstrating the practical feasibility of our approach.

As future development, we plan to modify the control of the ‘connectors’ in order to actively improve the connectivity (e.g., moving towards the center of the group or towards the closest ‘explorer’) and therefore decrease the overall completion time even more. Another extension could include imposing temporal targets that expire before any robot can possibly reach them. In our framework this could be easily achieved by letting the corresponding ‘prime traveler’ or ‘secondary traveler’ switching into a ‘connector’ whenever a target expires, for then automatically starting to explore the next target (if any).

An important direction worth of investigation would also be the possibility to (explicitly) deal with errors or uncertainties in the relative position measurements (w.r.t. robots and obstacles) needed by the algorithm. Indeed, the presented results rely on an accurate measurement of robot and obstacle relative positions obtained by means of an external motion capture system.

Another improvement could address the distributed election of the ‘prime traveler’ as was already discussed in Sec. 3.3. Indeed, while the adopted flooding approach does not require presence of a centralized planning unit, it still needs to take into account information from all robots. It would obviously be preferable to only exploit information available to the robot itself and its 1-hop

neighbors. This could be achieved by leveraging some (suitable variant) of the consensus algorithm as done for the decentralized propagation of the traveling efficiency of the current ‘prime traveler’.

## A Appendix

For the sake of completeness and readability, we will recap here the main features of the connectivity maintenance algorithm presented in Robuffo Giordano et al. (2013) with some small changes in the variable names. We start by defining  $d_{ij} = \|q_i - q_j\|$  as the distance between two robot positions  $q_i$  and  $q_j$ , and  $d_{ijo} = \min_{\varsigma \in [0,1], o \in \mathcal{O}} \|q_i + \varsigma(q_j - q_i) - o\|$  as the closest distance from the line of sight between robot  $i$  and  $j$  to any obstacle.

The main conceptual steps behind the computation of  $f_i^\lambda$  can be summarized as follows:

1. Define an auxiliary weighted graph  $\mathcal{G}^\lambda(t) = (\mathcal{V}, \mathcal{E}^\lambda, W)$ , where  $W$  is a symmetric nonnegative  $n \times n$  matrix whose entries  $W_{ij}$  represent the weight of the edge  $(i, j)$  and  $(i, j) \in \mathcal{E}^\lambda \Leftrightarrow W_{ij} > 0$ .
2. Design every weight  $W_{ij}$  as a *smooth* function of the robot positions  $q_i, q_j$  and of the obstacle points surrounding  $q_i$  and  $q_j$ , with the property that  $W_{ij} = 0$  if and only if at least one of the following conditions is verified:
  - (a) the maximum sensing range  $R_s$  is reached:  $d_{ij} \geq R_s$ ,
  - (b) the minimum desired distance to obstacles  $R_o$  is reached (where  $R_o < R_m$ ):  $d_{ijo} \leq R_o$ ;
  - (c) the minimum desired inter-robot distance  $R_c$  is reached:  $d_{ik} \leq R_c$  for at least one  $k \neq i$ .
3. Compute  $f_i^\lambda$  as the negative gradient of a potential function  $V^\lambda(\lambda_2)$  that grows unbounded when  $\lambda_2 \rightarrow \lambda_2^{\min}$  from above, where  $\lambda_2$  is the second smallest eigenvalue of the (symmetric and positive semi-definite) Laplacian matrix  $L = \text{diag}_{i=1}^n (\sum_{j=1}^n W_{ij}) - W$ , and  $\lambda_2^{\min}$  is a non-negative parameter. This eigenvalue  $\lambda_2$  is often also called Fiedler eigenvalue.

It is known from graph theory that a graph is connected if and only if the Fiedler eigenvalue of its Laplacian is positive (Fiedler 1973). If  $\mathcal{G}^\lambda(0)$  is connected, and in particular  $\lambda_2(0) > \lambda_2^{\min}$ , then under the action of  $f_i^\lambda$  the value of  $\lambda_2(t)$  can never decrease below  $\lambda_2^{\min}$  and therefore  $\mathcal{G}^\lambda(t)$  always stays connected.

From a formal point of view the anti-gradient of  $V^\lambda$  for the  $i$ -th robot takes the form

$$f_i^\lambda = -\frac{\partial V^\lambda(\lambda_2)}{\partial q_i} = -\frac{dV^\lambda}{d\lambda_2} \frac{\partial \lambda_2}{\partial q_i}. \quad (16)$$

Moreover, if the formal expression of  $V^\lambda$  and  $W$  are known then (16) can be analytically computed via the expression (Yang et al. 2010),

$$\frac{\partial \lambda_2}{\partial q_i} = \sum_{j \in N_i} \frac{\partial W_{ij}}{\partial q_i} (\nu_{2i} - \nu_{2j})^2, \quad (17)$$

where  $\nu_{2i}$  is the  $i$ -th component of the normalized eigenvector of  $L$  associated to  $\lambda_2$ .

In order to have a fully decentralized computation of  $f_i^\lambda$ , the robots perform a distributed estimation of both  $\lambda_2(t)$  and  $\nu_{2i}(t)$ , for all  $i = 1, \dots, N$ , as shown in Yang et al. (2010). In Robuffo Giordano et al. (2013) the authors finally prove the passivity (and then the stability) of the system w.r.t. the pair  $(f_i, v_i)$  for all  $i = 1, \dots, N$ , as well as the possibility to compute the connectivity force  $f_i^\lambda$  in (16) in a completely decentralized way.

## References

- G. Antonelli, F. Arrichiello, S. Chiaverini, and R. Setola. A self-configuring MANET for coverage area adaptation through kinematic control of a platoon of mobile robots. In *2005 IEEE/RSJ Int. Conf. on Intelligent Robots and Systems*, pages 1332–1337, Edmonton, Canada, Aug. 2005.
- G. Antonelli, F. Arrichiello, S. Chiaverini, and R. Setola. Co-ordinated control of mobile antennas for ad-hoc networks in cluttered environments. In *9th Int. Conf. on Intelligent Autonomous Systems*, Tokyo, Japan, Mar. 2006.
- T. Bektas. The multiple traveling salesman problem: an overview of formulations and solution procedures. *Omega*, 34(3):209–219, 2006.
- L. Biagiotti and C. Melchiorri. *Trajectory Planning for Automatic Machines and Robots*. Springer, 2008. ISBN 978-3540856283.
- W. Burgard, M. Moors, C. Stachniss, and F. Schneider. Coordinated multi-robot exploration. *IEEE Trans. on Robotics and Automation*, 21(3):376–386, 2005.
- J. W. Durham, A. Franchi, and F. Bullo. Distributed pursuit-evasion without global localization via local frontiers. *Autonomous Robots*, 32(1):81–95, 2012.
- J. Faigl and G. A. Hollinger. Unifying multi-goal path planning for autonomous data collection. In *2013 IEEE/RSJ Int. Conf. on Intelligent Robots and Systems*, pages 2937–2942, Chicago, IL, Sep. 2014.
- M. Fiedler. Algebraic connectivity of graphs. *Czechoslovak Mathematical Journal*, 23(98):298–305, 1973.
- A. Franchi, L. Freda, G. Oriolo, and M. Vendittelli. The sensor-based random graph method for cooperative robot exploration. *IEEE/ASME Trans. on Mechatronics*, 14(2):163–175, 2009.
- R. A. Freeman, P. Yang, and K. M. Lynch. Stability and convergence properties of dynamic average consensus estimators. In *45th IEEE Conf. on Decision and Control*, pages 338–343, San Diego, CA, Jan. 2006.
- V. Grabe, M. Riedel, H. H. Bülthoff, P. Robuffo Giordano, and A. Franchi. The TeleKyb framework for a modular and extendible ROS-based quadrotor control. In *6th European Conference on Mobile Robots*, pages 19–25, Barcelona, Spain, Sep. 2013.
- G. Hollinger and S. Singh. Multirobot coordination with periodic connectivity: Theory and experiments. *IEEE Trans. on Robotics*, 28(4):967–973, 2012.
- A. Howard, L. E. Parker, and G. S. Sukhatme. Experiments with a large heterogeneous mobile robot team: Exploration, mapping, deployment and detection. *The International Journal of Robotics Research*, 25(5-6):431–447, 2006.
- P. Jensfelt and S. Kristensen. Active global localization for a mobile robot using multiple hypothesis tracking. *IEEE Trans. on Robotics and Automation*, 17(5):748–760, 2001.
- J. Lächele, A. Franchi, H. H. Bülthoff, and P. Robuffo Giordano. SwarmSimX: Real-time simulation environment for multi-robot systems. In I. Noda, N. Ando, D. Brugali, and J.J. Kuffner, editors, *3rd Int. Conf. on Simulation, Modeling, and Programming for Autonomous Robots*, volume 7628 of *Lecture Notes in Computer Science*, pages 375–387. Springer, 2012.
- H. Lim and C. Kim. Flooding in wireless ad hoc networks. *Computer Communications*, 24(3-4):353–363, 2001.
- N. A. Lynch. *Distributed Algorithms*. Morgan Kaufmann, 1997. ISBN 1558603484.
- C. Masone, A. Franchi, H. H. Bülthoff, and P. Robuffo Giordano. Interactive planning of persistent trajectories for human-assisted navigation of mobile robots. In *2012 IEEE/RSJ Int.*

- Conf. on Intelligent Robots and Systems*, pages 2641–2648, Vilamoura, Portugal, Oct. 2012.
- V. Mistler, A. Benallegue, and N. K. M’Sirdi. Exact linearization and noninteracting control of a 4 rotors helicopter via dynamic feedback. In *10th IEEE Int. Symp. on Robots and Human Interactive Communications*, pages 586–593, Bordeaux, Paris, France, Sep. 2001.
- A. R. Mosteo, L. Montano, and M. G. Lagoudakis. Guaranteed-performance multi-robot routing under limited communication range. In *9th Int. Symp. on Distributed Autonomous Robotic Systems*, pages 491–502, Tsukuba, Japan, Nov. 2008.
- R. Murphy, S. Tadokoro, D. Nardi, A. Jacoff, P. Fiorini, H. Choset, and A. Erkmen. Search and rescue robotics. In B. Siciliano and O. Khatib, editors, *Springer Handbook of Robotics*, pages 1151–1173. Springer, 2008.
- T. Nestmeyer, P. Robuffo Giordano, and A. Franchi. Multi-target simultaneous exploration with continual connectivity. In *2nd Int. Work. on Crossing the Reality Gap - From Single to Multi- to Many Robot Systems*, at *2013 IEEE Int. Conf. on Robotics and Automation*, Karlsruhe, Germany, May 2013a.
- T. Nestmeyer, P. Robuffo Giordano, and A. Franchi. Human-assisted parallel multi-target visiting in a connected topology. In *6th Int. Work. on Human-Friendly Robotics*, Rome, Italy, Oct. 2013b.
- R. Olfati-Saber and R. M. Murray. Consensus protocols for networks of dynamic agents. In *2003 American Control Conference*, pages 951–956, Denver, CO, Jun. 2003.
- R. Olfati-Saber and R. M. Murray. Consensus problems in networks of agents with switching topology and time-delays. *IEEE Trans. on Automatic Control*, 49(9):1520–1533, 2004.
- F. Pasqualetti, A. Franchi, and F. Bullo. On cooperative patrolling: Optimal trajectories, complexity analysis, and approximation algorithms. *IEEE Trans. on Robotics*, 28(3):592–606, 2012.
- Y. Pei and M. W. Mutka. Steiner traveler: Relay deployment for remote sensing in heterogeneous multi-robot exploration. In *2012 IEEE Int. Conf. on Robotics and Automation*, pages 1551–1556, St. Paul, MN, May 2012.
- Y. Pei, M. W. Mutka, and N. Xi. Coordinated multi-robot real-time exploration with connectivity and bandwidth awareness. In *2010 IEEE Int. Conf. on Robotics and Automation*, pages 5460–5465, Anchorage, AK, May 2010.
- P. Robuffo Giordano, A. Franchi, C. Secchi, and H. H. Bühlhoff. A passivity-based decentralized strategy for generalized connectivity maintenance. *The International Journal of Robotics Research*, 32(3):299–323, 2013.
- E. Stump, A. Jadbabaie, and V. Kumar. Connectivity management in mobile robot teams. In *2008 IEEE Int. Conf. on Robotics and Automation*, pages 1525–1530, Pasadena, CA, May 2008.
- E. Stump, N. Michael, V. Kumar, and V. Isler. Visibility-based deployment of robot formations for communication maintenance. In *2011 IEEE Int. Conf. on Robotics and Automation*, pages 4489–4505, Shanghai, China, May. 2011.
- D. Tardioli, A. R. Mosteo, L. Riazuelo, J. L. Villarreal, and L. Montano. Enforcing network connectivity in robot team missions. *The International Journal of Robotics Research*, 29(4):460–480, 2010.
- P. Yang, R. A. Freeman, G. J. Gordon, K. M. Lynch, S. S. Srinivasa, and R. Sukthankar. Decentralized estimation and control of graph connectivity for mobile sensor networks. *Automatica*, 46(2):390–396, 2010.
- M. M. Zavlanos and G. J. Pappas. Potential fields for maintaining connectivity of mobile networks. *IEEE Trans. on Robotics*, 23(4):812–816, 2007.